STRUCTURE AND MECHANICS OF STRETCHED COLLAGEN FIBRILS

by

Chris Peacock

Submitted in partial fulfillment of the requirements
for the degree of Master of Science

at

Dalhousie University
Halifax, Nova Scotia
July 2019

This thesis is dedicated to my grandfathers William "Jackson" Peacock and Thomas "Dudley" Allan, for demonstrating to me the importance of humility and open-mindedness.

Table of Contents

List of Tables

List of Figures

Abstract

Collagen fibril are the smallest repeating units in load-bearing collagenous tissues such as tendon and bone, functioning as a microscopic stress mediators in mammalian bodies. These fibrils are twisted self-assembled aggregates of triple-helical polypeptides, forming with a characteristic 67nm density striation known as the D-band. Although the stress-strain curve of individual collagen fibrils has been studied, changes in the fibrillar structure with strain have typically been investigated through tissue-level measurements using X-ray scattering. In this thesis I address the need to mechanically and structurally assess individual collagen fibrils under tension by capturing atomic force images of collagen fibrils adsorbed to an elastomeric film (PDMS), which is strained using a house-build stretching stage. Results from this experiment show that the fibrillar structure responds inhomogeneously to applied tension through tautening and sliding of its constituent polypeptides, restructuring mechanisms that have been suggested in previous studies but never directly observed.

List of Abbreviations Used

AFM Atomic Force Microscope. 5

MEMS Microelectromechanical System. 11

PBS Phosphate Buffered Saline solution. 19

PDMS Polydimethylsiloxane. viii

PEG Polyethylene glycol. 6

QNM Quantitative Nanomechanical Mapping. 12

SAXS Small Angle X-ray Scattering. 8

SEM Scanning Electron Microscope. 11

TEM Transmission Electron Microscope. 12

Acknowledgements

I'd like to acknowledge my supervisor Laurent Kreplak for maintaining my enthusiasm and providing guidance throughout my studies. I'd like to thank Stephen Payne and Tanya Timmins for their tremendous efforts in keeping the Physics department operational. I'd also like to acknowledge Cameron Rudderham, Asif Iqbal, Fouad Kaadou, Patrick Strongman, Karan Chowdhry and all the others in the Dunn, room 207 and beyond for providing research advice and generally keeping life interesting.

Chapter 1

Introduction

1.1 Overview

Collagen is the most abundant protein type in mammals, and fulfills the role of maintaining the shape and the mechanical strength of tissue. The tissues with the highest collagen density in mammalian bodies exist within the skeletal structure or act as connective tissues between muscle and bone (such as ligaments and tendon). The tendon, being a model example of collagen's role as a stress mediator, has a structure that is self-similar at many length scales. Because of this, deformation mechanisms observed at the finest levels of the tendon structure can, through analogy, be related to those experienced by the tissue at the macroscopic level. The following sections describe briefly the hierarchy of tendon structure, including the role that the collagen fibril plays as the tissue's lowest-level constituent.

1.2 Tendon

Tendons are the primary load-bearing structural element in mammalian tissue. The function of a tendon is to mediate and transmit stress applied by muscle to the skeletal structure in mammals, and as a result the structure of a tendon is comparable to a rope or other woven synthetic fiber. Tendon tissues are unique in the animal kingdom in that they are composed primarily of a single molecular building block (type I collagen triple helixes); all other constituents (such as Proteoglycans [1] and Elastin [2]) of the tendon superstructure function to stabilize the tissue structure [3]. While the macroscopic shape and size of tendons varies between species and location within the body, tendons have a consistent hierarchical structure that ascends in length-scale as follows: collagen triple helical molecules ($\sim$1nm diameter) compose collagen fibrils ($\sim$100nm diameter) which compose fibers ($\sim 1\mu$m diameter) which compose fascicles ($\sim 100\mu$m diameter) which collectively form tendons (1-10mm diameter) [4].

The 'fascicle' echelon of tendon structure is sometimes broken into several sub-levels (primary, secondary and tertiary fiber bundles), with levels distinguished from one another by the presence of an endotenon membrane wrapping the fiber bundles [5]. This membrane laterally separates subcomponents of the tendon at multiple scales, so that axial stress dominates as the main mode of mechanical loading for these subcomponents (with axial stress observed to be 2-3 orders of magnitude larger than intrafibrillar shear stress when the tissue is loaded [6]).

1.3 Collagen fibrils in-vivo

The collagen fibril is the finest macromolecular structure within the tendon hierarchy. Just as the larger fibers and fascicles of the tendon structure are rope-like structures composed of smaller strands of collagen, the fibril is a twisted ply of triple-helical molecules [7] known as collagen trimers [8]. However because these triple-helixes are monomers in the context of fibril assembly, they will be referred to as *collagen monomers* going forward in this thesis. Type I collagen, the most common collagen-type found in tendon, consists of two $\alpha 1$ and one $\alpha 2$ procollagen chains. The pro-collagen chains are individually assembled in the interior of fibroblasts (cells that are responsible for synthesis of extracellular material in mammals) [9], and in the ($2\alpha 1$, $1\alpha 2$) proportion come together to form a helical structure stabilized by hydrogen bonding [10]. The triple helical procollagens terminate with a carboxyl group at one end and an amine group at the other (known as the C- and N- termini, respectively). At both the C- and N- termini of the newly-assembled procollagen monomer is a non-helical propeptide region [9]. Once assembled by the fibroblast, the procollagen monomer is ejected into the extracellular space, where C- and N- proteinase cleaves the C- and N-propeptide regions from the structure, respectively (figure 1.1) [11]. The cleavage of these domains transforms the procollagen into a collagen monomer (approximately 300nm in length) which goes on to aggregate with other monomers in a quasi-hexagonal packing [12] to form collagen fibrils. The formation of collagen fibrils from these monomers is a process of entropy-driven self assembly [5]; this makes the large-scale structure of the fibril sensitive to the morphology and amino-acid sequence of individual collagen molecules [13] [14] [15]. In the process of fibril assembly, the enzyme lysyl-oxydase binds to regions near the C- and N- termini of the collagen

monomers and catalyzes an oxydation reaction between the lysine and hydroxylysine residues of adjacent monomers. The product of this reaction is a 'zero-length' intermolecular cross-link, which further stabilizes the collagen fibril structure [16].

According to the Hodges-Petruska model of the fibrillar structure, Collagen monomers assemble within the fibril structure with a staggering of approximately $\frac{1}{5}$ of the distance between the like-termini of axially adjacent monomers [17]. This like-termini distance is longer than the monomer's 300nm length by ∼35nm; this distance is known as the 'gap' length. The gap spacing and axial staggering of molecules combined gives rise to a density striation with a length scale of $\frac{300+35}{5} \approx 67$nm and a low/high density ratio of 0.8 known as the *D-band*. The high and low density regions within the D-band striation are known as the *overlap* and *gap* regions respectively.

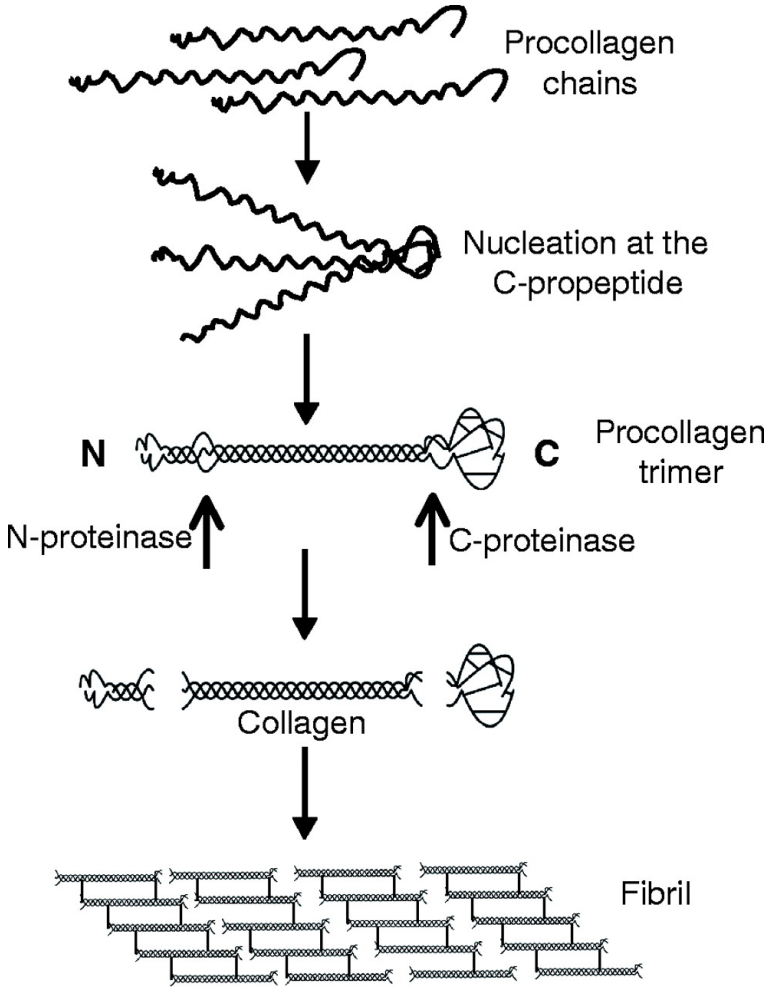

Figure 1.1: *An illustration of the fibril assembly process, from procollagen formation to molecular packing. Figure reprinted from [9]*

In addition to an axial density inhomogeneity, the collagen fibril super-structure has been observed to be helical ([18],[19]) with a pitch that varies between tissue type, but observed to be between 0.4 μm [20] and several microns. Modeling this structure as a double-twisted cylindrical liquid crystal, Cameron et al. suggest that the twisting of collagen molecules decreases the free-energy of fibril assembly [21], and that a radially-dependent twist angle works to limit the size of collagen fibril growth in-vivo. Furthermore the helical pitch of the collagen fibrils appears to be tissue dependent [20],[19]. This suggests that either the helical structure of fibrils provides tissue-level functionality, or that tissue-specific function influences the development of fibrillar pitch.

1.4 Fibrillar structure affects tissue mechanics

Macroscopic differences in mechanical properties between tissue types are, in part, manifestations of structural differences in their constituent collagen fibrils [22] [23]. A wide distribution of fibril radii, cross-link density and even sub-D-band structure have been observed across many species of the animal kingdom [24] [25] [26] [27]. Notably, collagen fibrils extracted from sea cucumber dermis have a unique transition region at their mid-point, where the N-C orientation of monomers flips to a C-N orientation. This, paired with a tapering of the fibril at its ends makes them resemble high-aspect-ratio spindles. There is evidence that even this tapering has a specific role in stress transfer in-vivo [28].

There can even be a large variety in fibril morphology within the same animal model. In their 2016 study, Herod et al. demonstrated that the bovine common digital extensor tendon is not only mechanically stronger than superficial digital flexor tendon extracted from the same animal, but that the failure mode of individual collagen fibrils from each tissue is distinct [22]. This is significant considering the difference in function between these two tissues; bovine extensor tendons provide cows with fine positional control of their hooves, whereas bovine flexor tendon stores and releases energy with every step the animal makes. In a single-fibril tensile testing experiment, Quigley et al. showed that collagen fibrils from these two tendon types have unique stress/strain behaviours and mechanical toughness, which speaks to the difference in function that these two tissue types have in-vivo [29] (figure 1.2). The mechanical

contrast between these two collagen fibril models can be in part attributed to their differences in intra-fibrillar cross-link density, which further dictates other structural-mechanical characteristics such as size [22] and fatigue resistance [30].

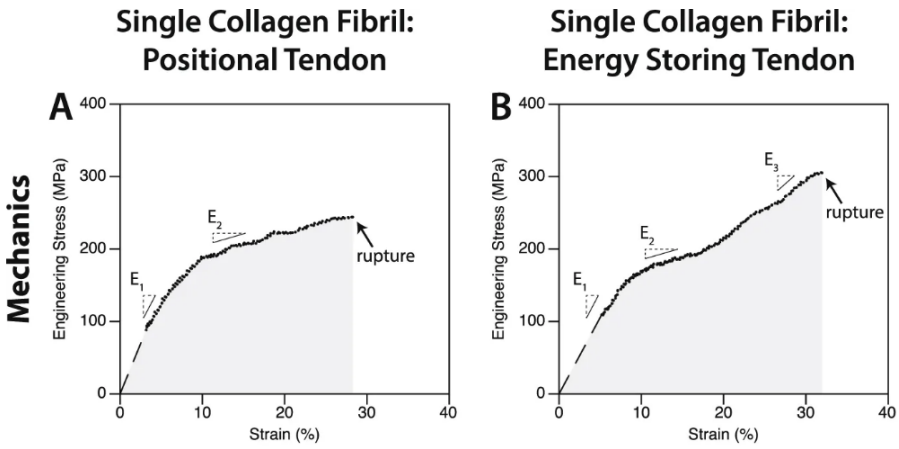

Figure 1.2: *a,b) Energy storing fibrils stiffen at high strain, while positional fibrils do not. The dashed line indicates the initial portion of the stress-strain curve that could not be captured using the bowstring technique, and was therefore approximated. Figure and caption reprinted from [29].*

1.5 Factors affecting the mechanics of collagen fibrils

Consistent with their function as a stress mediator in-vivo, collagen fibrils are famously robust under tension; depending on tissue type [31] [32] [33] and age, collagen fibrils are capable of withstanding 100s of MPa of applied axial stress before rupturing (see figure 1.2). There are a range of factors that affect fibril strength, below is a brief review of those that are relevant to this thesis.

1.5.1 Hydration

One of the most biologically relevant factors that affect fibril mechanics is hydration. Fibril water content has been shown to affect not only the strength of the fibril, but also its structure. In an Atomic Force Microscopy (AFM) based nanoindentation study, Andriotis et al. noticed that a ∼1.5-2 fold increase in fibril diameter corresponds to a decrease in indentation modulus of a full order of magnitude [34]. A single-microfibril molecular-dynamics simulation performed by Gautieri et al. suggests that

water acts as a lubricant within the fibrillar structure, pushing adjacent monomers apart and allowing them to slide across one-another [35]. Masic et al. demonstrated that water even has an effect on the conformation of collagen monomers, and that removing water from the fibril induces structural changes in the collagen triple-helixes which results in strong molecular tensile stresses [36].

Grant et al. tuned the modulus of hydrated collagen fibrils by bathing them with separate aqueous solutions of ethanol and monovalent salt [37]. The ethanol dehydrates the fibril by displacing water from within its structure [38], allowed for the reformation of inter-molecular hydrogen bonds. These bonds were unable to form when the water was present and screening the molecule-molecule interactions; their reformation has the effect of stiffened the fibril [37]. The salt has a similar effect on the hydration of the fibrils; increasing the concentration of solute in the solution surrounding the collagen fibril decreases the osmotic pressure between the interior of the fibril and the surrounding solution, thereby drawing water out from within the fibrillar structure [39]. Both treatments were found to increase the average indentation modulus of fibrils 2-3 fold. In a more recent experiment, Andriotis et al. dehydrated fibrils by immersing them in an aqueous solution of hydrophilic poly-ethylene-glycol (PEG) [34]. Their observations from this experiment were consistent with those made by Grant, while being cleaner by avoiding problems associated with salt crystallization and ethanol evaporation.

1.5.2 Intra-fibrillar cross linking

The collagen fibril structure is stabilized by inter-molecular cross-links, the most common of which form between lysine groups at the C- and N- termini of laterally adjacent molecules within the fibril. Development of these links is mediated by an enzyme known as lysyl-oxydase [40] [41]. These are known as *zero-length* cross-links, in that there is no tertiary species linking the two molecules together. There are also several types of 'true' cross-linkers present in mature collagen fibrils, the most common of which are Advanced Glycation End-products (AGE) [42]. AGEs are a family of intra- and inter-fibrillar cross-linking sugars which slowly accumulate in and around collagen fibrils as tissue ages. The accumulation of AGEs within the

collagenous matter reduces the viscoelasticity of collagenous matrices [43]. Curiously, the density of AGEs cross-links within the fibrillar structure has a negligible effect on the mechanical properties, only affecting the mechanisms by which the fibril deforms at high strain [44] [45].

The density and distribution of intra-fibrillar cross-linking affects the viscoelasticity of individual collagen fibrils [44] [42]. This causes the mechanics and structure of collagen fibrils to be dependent on the fibrillar strain rate, and they furthermore contribute to the 1-2 minute relaxation time of the collagen fibril after strain has been applied [46].

1.6 Ligand-collagen interactions in-vivo

The main function of collagen in tissue, either in a hierarchical super-structure such as tendon or in the extracellular matrix, is to mediate stress. Cells use matrices of collagen fibrils to transmit mechanical signals over short distances, as well as to move and re-orient themselves in tissue. For instance, cells have been observed to align perpendicular to the direction of strain in tissue [47], presumably to avoid being stretched along with the collagenous network. Functional binding sites for various species of ligand (such as integrin, used by cells to bind to collagen) are unevenly distributed along the length of collagen monomers; Wang et al. have observed that a majority of the ligand binding sites exist within a distance of $\frac{1}{3}$ of the full length of the monomer from its C-terminus [48]. Ligand binding is therefore quite sensitive to the exposure of binding sites along the length of the α-triple helices [49], which is affected by the helix's conformation and by their assembly into the fibrillar structure [50]. As an example: Matrix Metaloproteinase (MMP) is a family of enzymes which mediate proteolysis of collagen triple helixes. In human molecular collagen, several species of MMP are known to bind at a thermally labile site near the C-terminus of the triple helix [51]; a site which is partially occluded by adjacent molecules when built into the fibrillar structure [49].

However, the structure of the collagen fibril is not static but is in a constant state of structural reorganization, which may provide brief opportunities for ligands to bind to the fibril at locations otherwise buried in the fibril [52] [53]. Applying stress to the fibrillar structure likely causes the conformation of collagen monomers to change,

potentially affecting binding site exposure and the modes of dynamic restructuring of the fibril. However, there are currently no experiments in the literature that have stabilized the structure of a strained, hydrated collagen fibril, and so the effects of strain on ligand binding is entirely speculative at this time.

1.7 Micro- and nano-mechanical testing of collagenous tissue

Tensile tests have been performed on collagenous material at a range of length scales, the most common and anatomically relevant being tests performed on whole tendons [54] [55] [56]. However, in the last 2 decades there has been a developing interest in the structural changes induced in collagen fibrils by applied strain. Here a brief review of the more recent fibrillar straining methods.

1.7.1 Measuring fibrillar strain through application of tissue-level stress

X-ray scattering is a common tool used to quantify structural changes on the fibrillar level, in tissue-straining experiments [57] [58]. This is a non-destructive technique where the intensity of X-ray light scattered from a sample is monitored (typically as a function of scattering angle) to determine the material's molecular structure, averaged over the entire sample. Using this approach, changes in the fibrillar structure can be monitored in real-time as a function of tissue level strain using the scattering patterns obtained through X-ray scattering. This technique was used on a rat-tail tendon by Fratzl et al. to demonstrate that only about 40% of strain applied on the tissue level is transmitted to the constituent fibrils (figure 1.3), and that the transmission begins at the start of the linear regime of the tendon stress-strain curve (after the tauting of fascicles and fibers within the tendon structure) [59].

Because X-ray scattering patterns can be obtained continuously while tensile tests are performed on tissue, the time-dependent response of the fibrillar structure to strain can be quantified using this technique. Recently Screen et al. were able to capture the relaxation behavior of fibrils immediately after applying tension to tissue, making a model-based statement that collagen fibrils experience morphological changes induced by water leaving/entering the fibrillar structure, post-stress application [60]. Currently, SAXS-based tendon tensile testing is the only method capable of capturing such time-dependent structural changes. However, the patterns obtained from

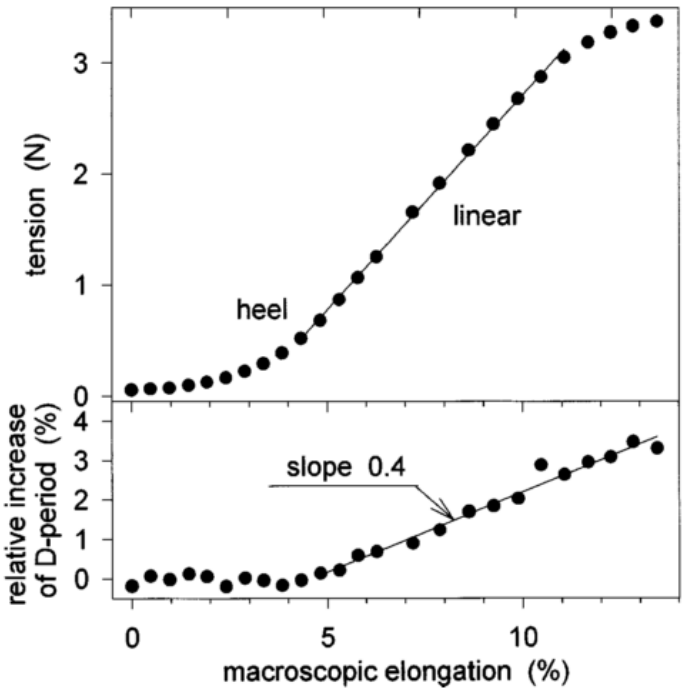

Figure 1.3: *Tension required for the elongation of a rat tail tendon (top) and corresponding average collagen fibril D-band strain (bottom). Figure and caption reprinted from [59]*

X-ray scattering provide only an average picture of how the fibrillar structure evolves with strain, and analysis of these patterns relies on modeling the system of interest with a simplified geometry (such as a uniform distribution of cylinders [42] [58]). Furthermore, the peaks in the X-ray scattering intensity associated with the D-band density striation have been seen to disappear after ∼5% D-band strain, which means evaluating the fibrillar structure beyond this threshold is effectively not possible [42]. In lieu of this limitation, various single-fibril straining methods have been introduced that sacrifice sample size for greater detail of the single-fibril strain response.

1.7.2 Review of previous single-fibril straining methods

Several unique techniques have been used to strain individual collagen fibrils. A large portion of the literature on straining individual fibrils and collagen molecules is dedicated to techniques that separate the straining procedure from subsequent nano-structural/mechanical assessment [61] [62] [63] [64]. A popular straining method

known as *nanofishing* involves attaching one end of a collagen fibril to a glass substrate and the other end to an AFM cantilever, and obtaining a stress/strain relationship by retracting the cantilever from the surface at a constant rate and measuring its deflection as a function of retraction distance (see figure 1.4).

In the studies performed by Graham and van der Rijt and coworkers, subsequent structural analysis of the fibrils post-strain was entirely omitted, and so the mechanisms by which the deformation occurred were speculative, based on features in the force-extension curves [61] [63]. Quigley et al. introduced a novel approach to straining collagen fibrils by pulling on sections between glue-points with an AFM cantilever, similar to the drawing back of a bow [23]. Using this technique, post-straining analysis could be performed immediately after tensile testing (as the AFM cantilever was not fixed to the collagen fibril with glue, as has been the case in previous studies). However, as with the nanofishing studies it was only possible to investigate the deformed structure of the collagen fibril after stress had been applied and subsequently removed.

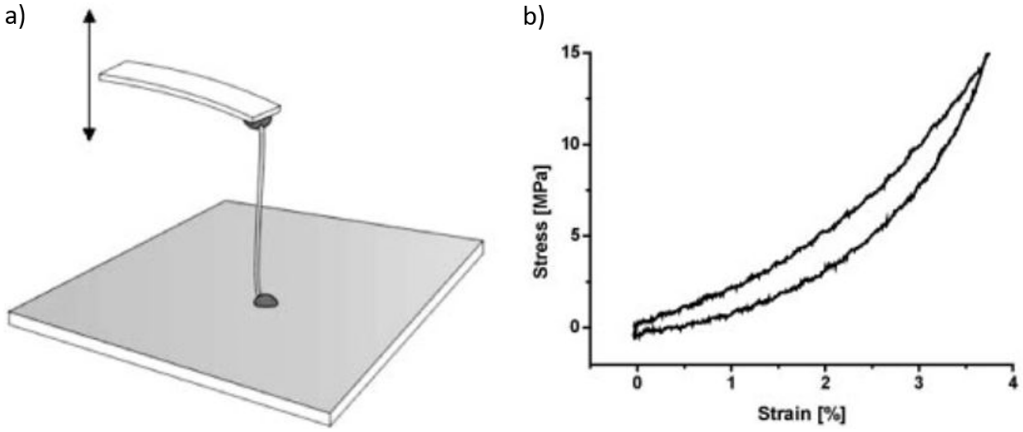

Figure 1.4: *a) An illustration of the AFM-based nano-fishing method of tensile testing, applied to a single collagen fibril. b) An exemplary stress-strain curve for a single fibril, both in extension and on return. Figure reprinted from [61].*

In a similar vein, optical tweezers have been used to perform force spectroscopy on collagen fibrils as well as on individual collagen monomers [65] [66]. As with the AFM-based force spectroscopy methods discussed above, optical tweezers obtain the stress-strain relationship for individual collagen fibrils but fail to capture the mechanism by which the fibrillar structure deforms with extension. Furthermore,

this technique is limited to the application of force in the pico-newton range, as opposed to the nano- to micro-newton capabilities of nanofishing. Shen et al. used a MEMS device to perform tensile tests on individual collagen fibrils (figure 1.5) [46]. Using a simple Maxwell-Weichert spring-dashpot model, they were able to recognise two distinct relaxation times from the recorded stress-strain curves, one occuring on a short timescale (7 ± 2s) and another longer relaxation time (105 ± 5s). All the previously mentioned single-fibril stretching techniques suffer from the localization of stress at the clamping-points on the collagen fibril; this detail further complicates interpretation of the fibrillar stress-strain relationship obtained using these methods.

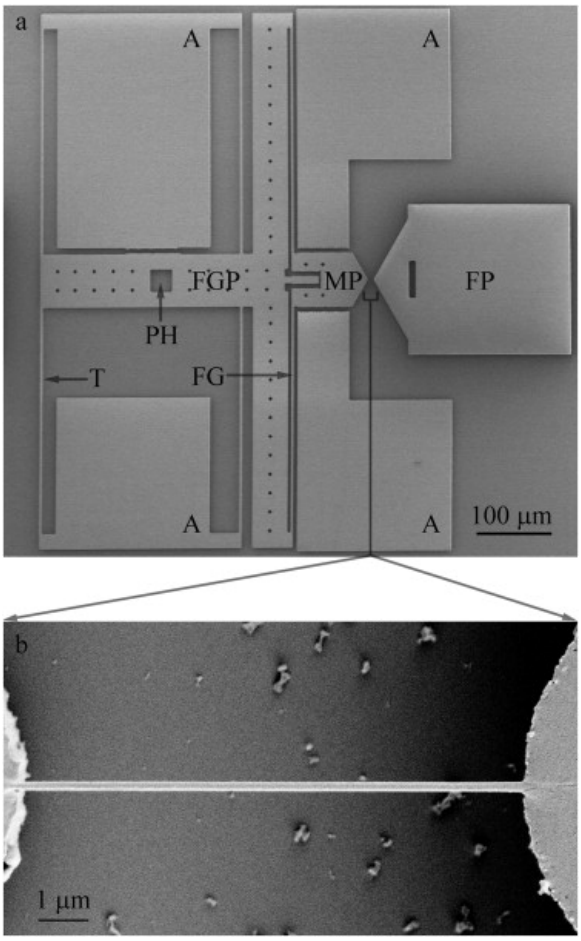

Figure 1.5: *A SEM image of the MEMS device used by Shen et al. to strain individual collagen fibrils. Figure reprinted from [46]*

Several in-silico studies have been performed to simulate the strain-response of individual fibrils and collagen monomers. The most prevalent work in the field has

been performed by members of Buehler's group, who in the last decade have modeled strain-rate-dependent structural changes in strained collagen molecules, the dependence of hydration on fibril and molecule [67] [68] strain response, as well as the effects of mineral content [69] and cross-link density [70] on the deformation mechanisms of fibrils. Results from many of these studies are in excellent agreement with previous (and subsequent) studies of strained collagen fibril.

1.7.3 AFM nano-indentation applied to collagen fibrils

Atomic force microscopy remains one of the only techniques capable of directly resolving D-band-level structural details in collagen fibrils. As an imaging modality it also has the advantage over SEM and TEM of capturing topographical and mechanical details of collagen fibrils rather than just electron density. As opposed to EM or confocal microscopy-based techniques, AFM requires no metal coating or fluorescent labeling to capture images, making it a (relatively) non-invasive means of capturing sub-micron structural information.

Several AFM imaging modalities exist, each with their relative advantages in particular applications [71]. The most common imaging mode is known as *tapping mode*, which is an intermittent contact mode where the cantilever is driven to oscillate at/near resonance and atomic force measurements are made using phase shifts and changes in the amplitude of this motion as the probe scans the sample [72]. Using tapping mode, Gutsmann et al. demonstrated that collagen fibrils may be radially inhomogeneous in density, further suggesting that the fibril structure may be comparable to a hollow tube rather than a woven rope [64].

Contact imaging modes, such as *Force volume* and *Quantitative Nanomechanical Mapping* modes, operate by oscillating the cantilever at a sub-resonance frequency and uses the probe as a sample indenter. These modes obtain mechanical information from the sample of interest by recording applied indentation force as a function of cantilever displacement for each indentation, and fitting these curves to an indentation model from classical elasticity theory. Using the force volume mode, Grant et al. were the first to demonstrate that water content in hydrated collagen fibrils dramatically affects their radial indentation modulus [37]. A comparable and more recent method to force volume (known as Peakforce Quantitative Nanomechanical Mapping (QNM))

was used by Baldwin et al. to capture nanomechanical maps with a <10nm/pixel resolution [73]. In this study, Baldwin demonstrated that the speed at which the indentation is performed affects the indentation modulus measured on collagen fibrils, further demonstrating the viscoelastic properties of the fibrillar structure. When indenting the fibril at a sufficiently high speed (∼1.2mm/s) the indentation modulus contrast between the gap and overlap regions of the fibril's D-band repeat was observed to be comparable to the gap-overlap density ratio of 0.8 predicted by the Hodges-Petruska stacking model [17]. The interpretation from Baldwin et al. was that as long as the indentation speed remains faster than the shortest viscoelastic relaxation time of the fibril, the structure will not have time to relax between indentations and so the modulus becomes a proportional to molecular density.

Atomic force imaging can been paired with tensile testing to make topographical measurements on collagen fibrils as a function of fibrillar strain. Inspired by the stretching of cells on elastic substrates [74], Wenger et al. adsorbed collagen fibrils to a sheet of silicone rubber and strained them by stretching the substrate [75]. This approach of straining collagen fibrils avoids the stress-localization problems associated with previous single-fibril straining methods, and at the same time stabilizes the strained fibrillar structure for structural assessment. Subsequent to strain application, the adsorbed fibrils were dried and morphological changes in the collagen fibrils were measured using an AFM operating in tapping mode. This was the first study to directly measure structural changes in collagen fibrils as a function of D-band strain, and it is this study that inspired the experiment performed during my thesis.

1.8 Current work and research questions

From my review of the literature on straining collagen fibrils, I identified a need to elucidate directly the mechanical-structural response of collagen fibrils in the process of being strained. The following are 2 research questions which I hoped to answer with a series of experiments:

1. Gautieri, in their SAXS- based study of strained collagen fibrils, make a model-based claim that the gap and overlap regions experience different amounts of strain when the D-band period elongates [42]. Can this strain inhomogeneity be observed

directly by imaging individual fibrils at several increments of applied strain?

2. The maximum D-band strain observed in SAXS-based experiments is 5% [42]. Is the D-band length measurable beyond 5% strain using a direct imaging method? If so, does the fibril structure deform irreversibly or fail beyond 10% D-band strain as suggested by Depalle et al.'s in-silico work [76]?

Using an AFM operating in the Peakforce QNM imaging mode used by Baldwin et al. [73], I attempted to answer these questions by measuring the nanomechanical properties of collagen fibrils as a function of strain. This was done using a substrate strain-transmission method inspired from work by Wenger et al. [75].

Chapter 2

Materials and Methods

2.1 Overview

This section describes in detail an experiment developed to monitor the structural and mechanical changes of a single collagen fibril as a function of applied strain. An overview of the sample preparation process is illustrated in figure 2.1.

2.2 Sample preparation

All samples prepared in this study were sourced from a single common digital extensor tendon. This tendon was collected from the forelimb of an 18-24 month old steer at a local slaughterhouse (Oulton farm, Nova Scotia, Canada) and immediately frozen in a -80°C freezer. Before each experiment, a 2mm section of the extensor tendon was sliced from the full tendon and allowed to defrost in a petri dish for 5 minutes. The defrosted sample was hydrated with 200μL deionized water before being manually splayed with a razor blade and tweezers to release collagen fibrils into the surrounding water. 60 μL of the water-collagen solution was pipetted onto the surface of a 1cm$\times$3cm strip of 200μm-thick PDMS (Electron Microscopy Sciences, USA) that was clamped into a motorized stretching stage. Collagen fibrils suspended in the droplet were allowed to settle to the surface of the PDMS for 1 hour, to which they strongly adsorbed. After the settling period, the drop was removed with a pipette and the PDMS film was washed with a steady stream of several hundred μL of fresh deionized water. The sample still mounted on the stretching stage was left to desiccate overnight, approximately 18 hours before imaging.

Through a series of deposition trials, I found that pipetting 10-12 5μL droplets in a grid-pattern resulted in a more uniform distribution of adsorbed fibrils than what was observed from the single droplet deposition. The difference in fibril distribution

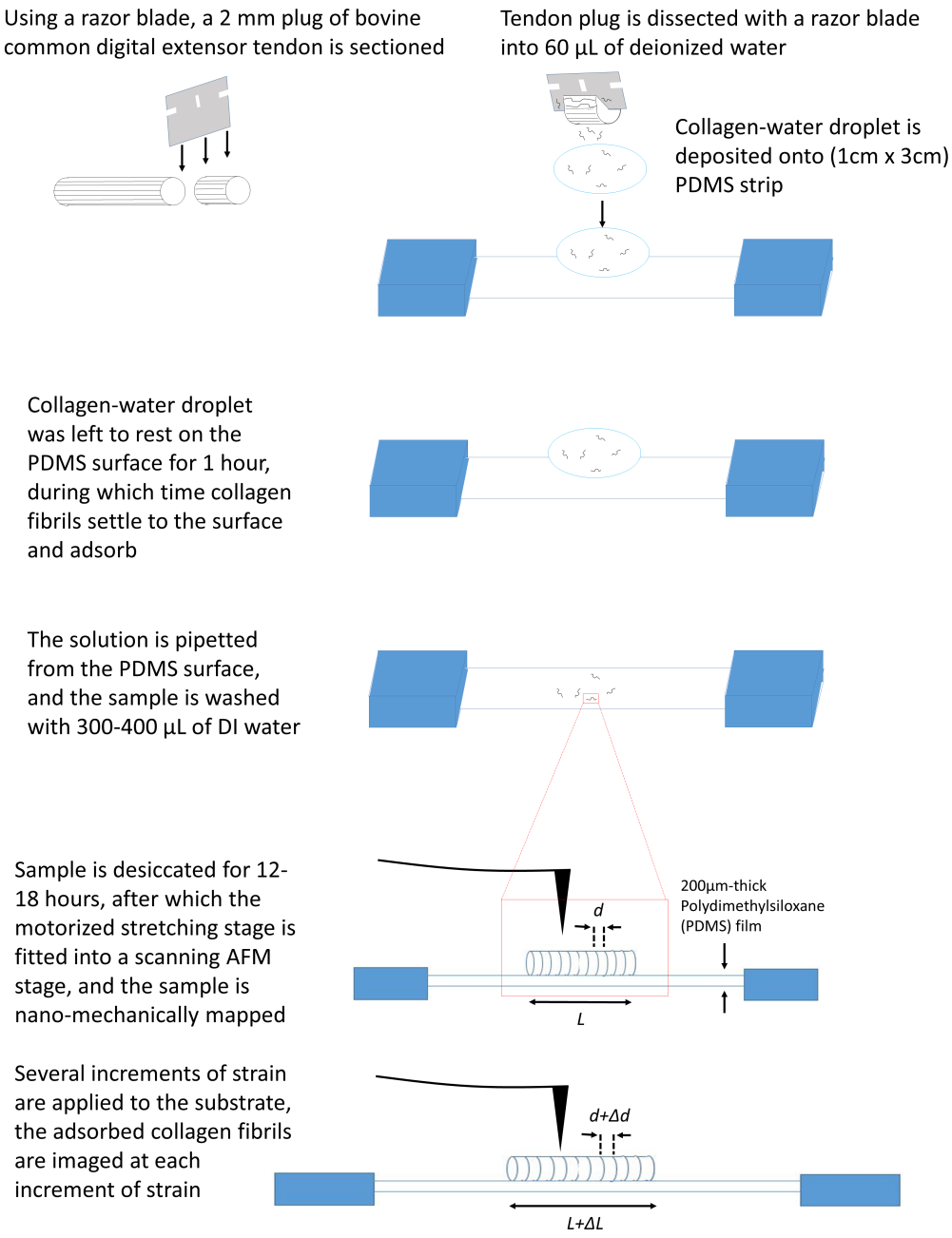

Figure 2.1: *Sample preparation procedure*

between these two methods can be attributed to the coffee ring effect, where material suspended in a drop sediments to the outer perimeter of the drop as it dries. When liquid evaporates from the surface of each drop, there is a net radial flux of liquid

carried from the interior of the droplet to replace the evaporated liquid at the surface. This flow carries suspended collagen fibrils to the droplet surface, which eventually settle to the drop perimeter due to gravity. By depositing a grid of small droplets on the PDMS, the magnitude of this bulk-to-perimeter displacement is small compared to that of fibrils deposited from a larger droplet. With only a single $60\mu L$ droplet, fibrils originally suspended in the droplet bulk are often deposited outside of the field of view of the visible light microscope, making them inaccessible to the AFM cantilever for imaging. Although the droplet grid method resulted in a larger number of fibrils within the microscope field of view than the single droplet method, the choice of deposition method had no observable effect on the adsorption of individual fibrils to the PDMS surface. Therefore, the two methods were used interchangeably in this study and will not be distinguished further in the experimental method.

2.3 Bruker SCANASYST fluid+ probe calibration

The SCANASYST Fluid+ cantilevers used in AFM imaging were calibrated by performing a 500nm ramp of the probe to the surface of a dry glass microscope slide. The vertical displacement of the laser on a four-quadrants photodiode was measured as a function of the Z-piezoelectric element position, a line was fit to the linear displacement-indentation regime of this curve to extract a deflection sensitivity (in nm/V). The cantilever was then removed $500\mu m$ from the surface of the glass slide, after which the thermal tune method introduced by Sader et al. was applied to calculate the deflection spring constant (in N/m) for the cantilever [77]. In this process, the cantilever is left to oscillate in response to the thermal noise of the air surrounding the cantilever, and the first fundamental frequency peak of the resulting power spectrum was fit with a Lorentzian function. Typical values for the deflection sensitivity, first fundamental frequency and cantilever spring constants were 13±1.6 nm/V, 129±1 kHz and 0.9±0.2N/m respectively. These three quantities are the mean ± standard deviations of values obtained from calibrating n = 35 separate atomic force cantilevers. All measurement were within the range of calibration estimates advertised by the manufacturer.

2.4 Tensile testing stage

2.4.1 Design of the mechanical stretching stage

The stretching instrument was constructed to be a low-profile and lightweight vertical extension to the sample holder present on the stage of an Atomic Force Microscope (Bioscope Catalyst AFM; Bruker, USA). Two motorized stages (National Aperture MM-1M) were attached to a machined block of aluminum (Appendix A.1) and a set of aluminum motor clamps (Appendix A.2) were attached to the moving stages of each motor. A 2cm-diameter hole was drilled through the extension between the motors perpendicular to the axis of travel of the motor stages, to allow clearance for a long working distance 20× objective mounted on a IX71 inverted visible light microscope (Olympus, USA). The procedure for operation is as follows: a 1cm×3cm strip of PDMS with adsorbed collagen fibrils on its surface is clamped between the two motors. The atomic force microscope head is placed on a set of aluminum stilts (Appendix A.3) to make room for the stretching stage beneath, and the cantilever is lowered to the surface of the PDMS to capture images. In order to avoid exciting an oscillatory mode in the suspended PDMS strip while scanning with the cantilever, a $200\mu m$-thick microscope cover slide is held to the underside of the PDMS and clamped in this position with a side-clamp (Appendix A.4). This entire clamp assembly is depicted in Appendix A.5.

2.4.2 Calibration of the mechanical stretching stage

A $30nm$ thick layer of gold was deposited onto the surface of a PDMS strip through a hexagonal lithography mask (8GC360 TEM grid, Sigma Aldrich, USA). This treatment patterned the surface of the strip with a grid of hexagons with a like-vertex spacing of 60μm (figure 2.2a). The hexagonal pattern served as a grid of fiducial points to estimate the strain field of the PDMS surface as the film is stretched by the motors. Using the inverted microscope, distances between like vertexes of neighboring hexagons was measured as a function of strain applied simultaneously by the two motors. Starting with the PDMS strip pulled taut between the two clamps, six increments of 5% strain were applied to the sample. The PDMS strip was extended from an unstrained length of 23.7mm at an extension speed of 50μm/s (25μm/s for each

motor, corresponding to a strain rate of 0.2%/s). At each 5% strain increment five measurements of hexagon-hexagon distance were recorded and averaged (figure 2.2a). Average hexagon-hexagon distance strain values are plotted versus film strain applied (figure 2.2b). The measured strain was systematically smaller than the applied strain, for applied strain increments above 15%.

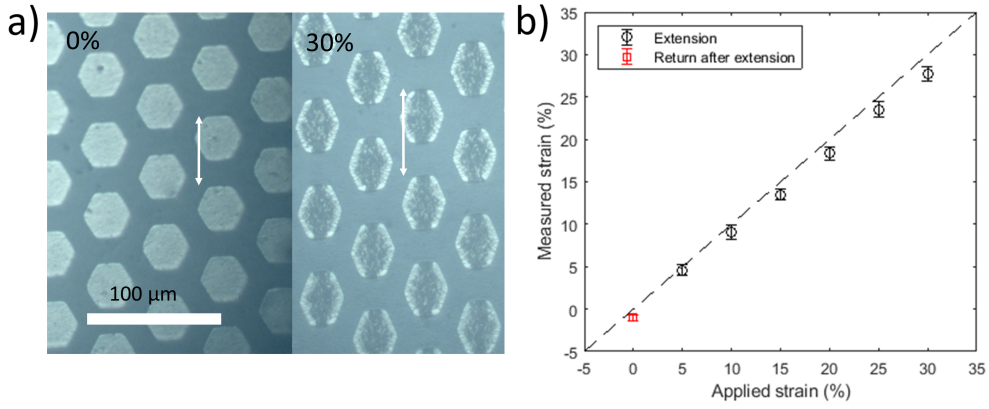

Figure 2.2: *a) Gold hexagons deposited on an unstretched PDMS strip versus hexagons on the PDMS strip that has been strained by 30%. b) Inter-hexagon distance strain versus total PDMS film strain. The dotted line indicates a 1:1 correspondence between applied and measured strain.*

2.5 Fibrillar extension tests

2.5.1 AFM imaging

All AFM images were obtained in 1× Phosphate buffered saline (PBS) using a Bioscope Catalyst (Bruker, USA) operating in Peak Force Quantitative Nanomechanical Mapping mode (Peak Force QNM). The images were 256×256 arrays obtained at a vertical tip velocity of 1.2 mm/s, a scan rate of 0.5 Hz, a peak force amplitude (oscillatory amplitude) of 300nm and a peak force set-point of 5 nN. Force versus distance curves were acquired at every pixel.

2.5.2 Fibril straining procedure

Dessicated samples were re-hydrated with 60μL of PBS for about 30 minutes before imaging began. AFM imaging was performed while the PDMS strip was held between

the clamps of the motorized stage extension, and a microscope slide was clamped beneath the PDMS to support the sample for imaging. An inverted visible light microscope (IX71, Olympus, USA) was used to find 50μm long fibrils that were oriented along the stretching axis, to be centered under the cantilever for imaging.

An initial low resolution image (256×256 pixel with dimensions 50μm×50μm) was captured to find the position and conformation of the fibril on the PDMS substrate and to extract its contour length. Three consecutive high resolution images (256×256 pixel, 2μm×2μm) were then taken in a region near the center of the fibril's length, such that the three images overlapped by approximately 200nm at the image's edges. This was done to ensure that a continuous 5-6μm segment of the fibril was captured between the three regions. Capture of all 4 images took approximately 1 hour on average per fibril.

After the imaging of each fibril, the PBS solution was removed from the sample and washed with 60μL deionized water three times before 60μL of fresh PBS solution was deposited once again onto the sample. This was done to avoid the build-up of excess salt as the solution evaporated during imaging. The glass microscope slide and crossbar clamp were removed and the motorized clamps strained the sample by a 5% increment. The microscope slide and crossbar clamp were then re-installed and the imaging procedure was repeated. Imaging began about 10 minutes after strain was applied, which exceeds the relaxation time of single fibrils of approximately 100s [46]. The sample was returned to its original length from a maximum of 30% strain in one increment and subsequently imaged using the same method as described above.

2.6 Data analysis

2.6.1 Fibril contour length

To estimate the strain applied to each collagen fibril, a Matlab-based software [78] was used to extract contour lengths of collagen fibrils from the 50μm×50μm low resolution images captured at each applied strain. A *fiducial length* was measured as the length of fibril section between fiducial markers on the PDMS background. The

most common of these markers were micron-sized chunks of biological matter, that remained adhered to the PDMS after the sample rinsing process. The procedure for extracting contour length is the following: the 50μm $\times$ 50μm height image is binarized by using a half-maximum threshold, followed by skeletonizing the image to convert the fibril to a 1-pixel-wide line. A series of cubic splines were then fit to the section of this line between two fiducial markers in the field of view. The arc length of the spline series was calculated and converted from pixel length to true length using the factor ($50\mu m$/256pixels = 195nm/(pixel). For an illustration of this process, see figure 2.3. The fiducial points used to measure this length were always chosen such that the 2μm$\times 2\mu$m regions of interest were included between the points, so that changes in this measurement are indicative of fibrillar strain within the high-resolution $2\mu m\times$ $2\mu m$ images.

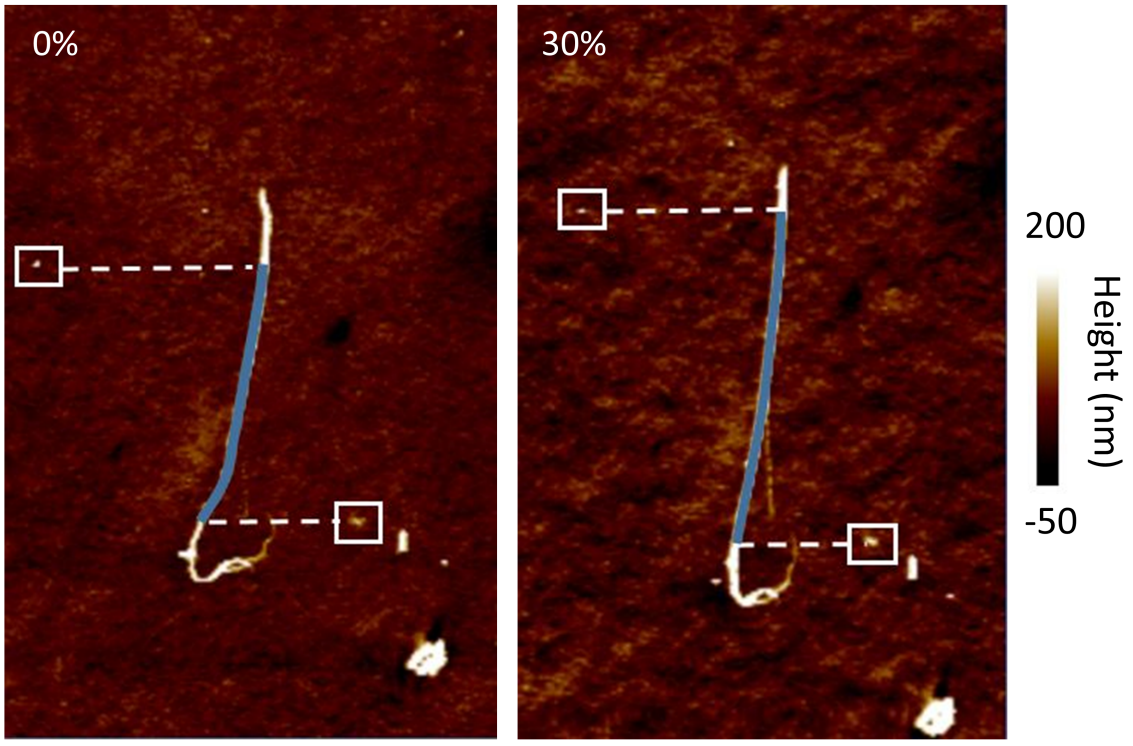

Figure 2.3: *Fiducial strain is measured as the change in length of a section of the fibril measured between two fiducial markers.*

2.6.2 Indentation modulus

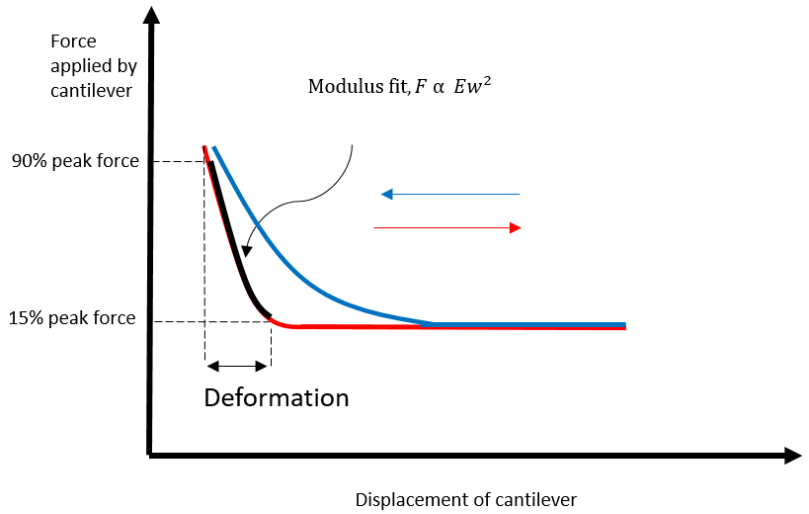

Figure 2.4: *Diagram depicting the typical shape of a force curve obtained through indenting a collagen fibril. Extraction of the indentation modulus and deformation are also demonstrated in this diagram.*

When the AFM cantilever indents the sample, a force versus cantilever displacement curve is captured both for the forward indentation and reverse retraction of the tip from the sample. From the retraction portion of this force-indentation curve, an *indentation modulus* is calculated by fitting the portion of the curve between 15% and 90% of the maximum applied indentation force (0.75nN and 4.5nN, for the maximum indentation of 5nN used here) to equation 2.1 [79]. This equation is the Sneddon indentation model for a conical indenter of half angle α displaced a distance w into a uniform and isotropic half-space with elastic modulus E. Poisson's ratio σ was set to 0.5 here, to be compatible with previous studies [73]. The cantilevers used here have an approximate half angle of 18°, with a nominal tip radius of 2nm.

$$F = \frac{2E\tan(\alpha)}{\pi(1-\sigma^2)}w^2 \tag{2.1}$$

The PeakForce Quantitative Nanomechanical Mapping imaging mode captures a 256-point force-curve at each pixel of an image. Limited to a maximum resolution of 256×256, these images have the shape of a 256×256×256 data-cube before any post-processing is applied. Indentation modulus maps are generated from the captured force-curve image volumes by performing the curve fitting described above.

The indentation modulus captured using PeakForce QNM can be used as a proxy for local molecular density, an interpretation originally made by Baldwin and coworkers in their 2014 work [73]. With this in mind, the periodic contrast in modulus along the length of the collagen fibril in figure 2.5 is representative of the D-band density striation. Combining nanomechanical mapping with this straining method therefore allows for the monitoring of local density changes in the fibrillar structure as a function of applied fibrillar strain.

The peak indentation force was held at a constant 5nN throughout this series of experiments. Force curves obtained from samples with elastic modulus higher than 70MPa tended to reach this 5nN peak force after only 1-5nm indentation depth. Using a peak force amplitude of 300nm, this indentation depth corresponds to just 2-3 force measurements before peak force is met. This low number of points to fit equation 2.1 to leads to an inaccurate estimation of the indentation modulus. Therefore, indentation modulus measured to be above 70MPa using this procedure were considered untrustworthy, and as an alternative the deformation was used as a proxy for sample stiffness.

2.6.3 Deformation

Deformation is measured as the difference in Z-piezo position between the 15% maximum force measurement and the peak force measurement, obtained from the retraction portion of the force curve. It is therefore a measurement of tip indentation depth, combined with the deflection of the cantilever. In their pioneering study investigating the nanomechanical properties of single collagen fibrils, Baldwin and coworkers demonstrated that deformation measurements made using Peakforce QNM are inversely proportional to indentation modulus [73]. This inverse relationship is represented in figure 2.6. As discussed in section 2.6.2, these indentation modulus measurements are over-estimated when indenting stiff samples with a low peak force. To avoid this effect it is useful to monitor both deformation and indentation modulus, using inverse deformation as a more reliable measure of sample stiffness in >70MPa sample elastic modulus regime. In addition, deformation is a proxy to sample stiffness that is not model dependent, and is obtained in real time during imaging without any post-processing.

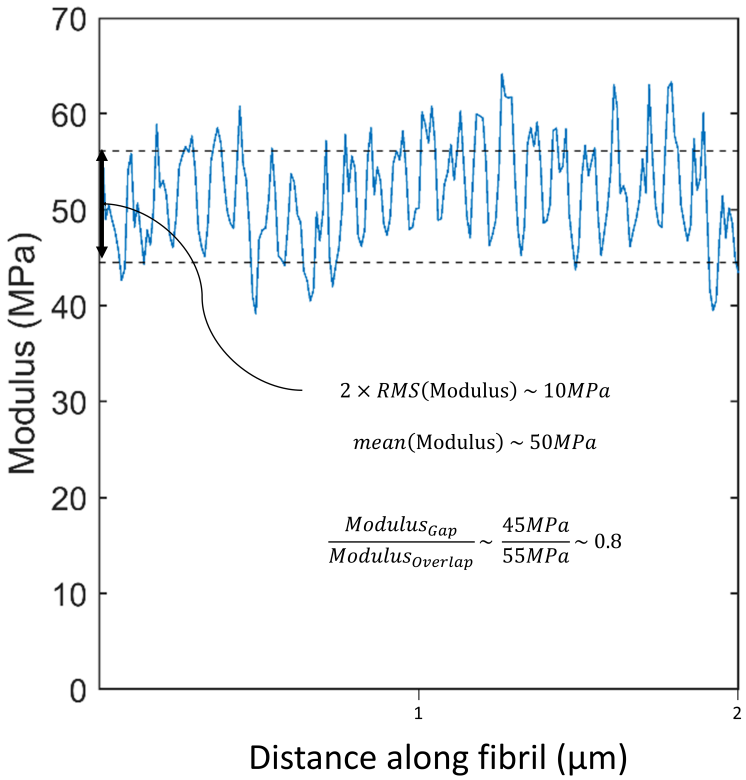

Figure 2.5: *An example of how the 4:5 density contrast between the gap and overlap regions of a collagen fibril is captured in the indentation modulus image.*

However, because deformation is measured in the contact regime of the force curve, it is quite sensitive to the error in peak force between individual curves. Sudden changes in sample topography lead to large errors in the peak force; these lead to edge effects which appear as sharp peaks in the deformation image.

2.6.4 Fibril height

The sample height is measured as the difference between the Z-piezo setpoint value measured when the cantilever first engaged the sample's surface and the setpoint measurement at the point of interest. However, as this height measurement is made when the tip has reached the peak force setpoint value, it is therefore a measurement of the tip position after indentation rather than the position of the tip at first sample contact prior to indentation. To obtain the latter from the former, Baldwin and coworkers added the deformation and height images together, using the deformation measurements as pixel-by-pixel correction factors for their corresponding height

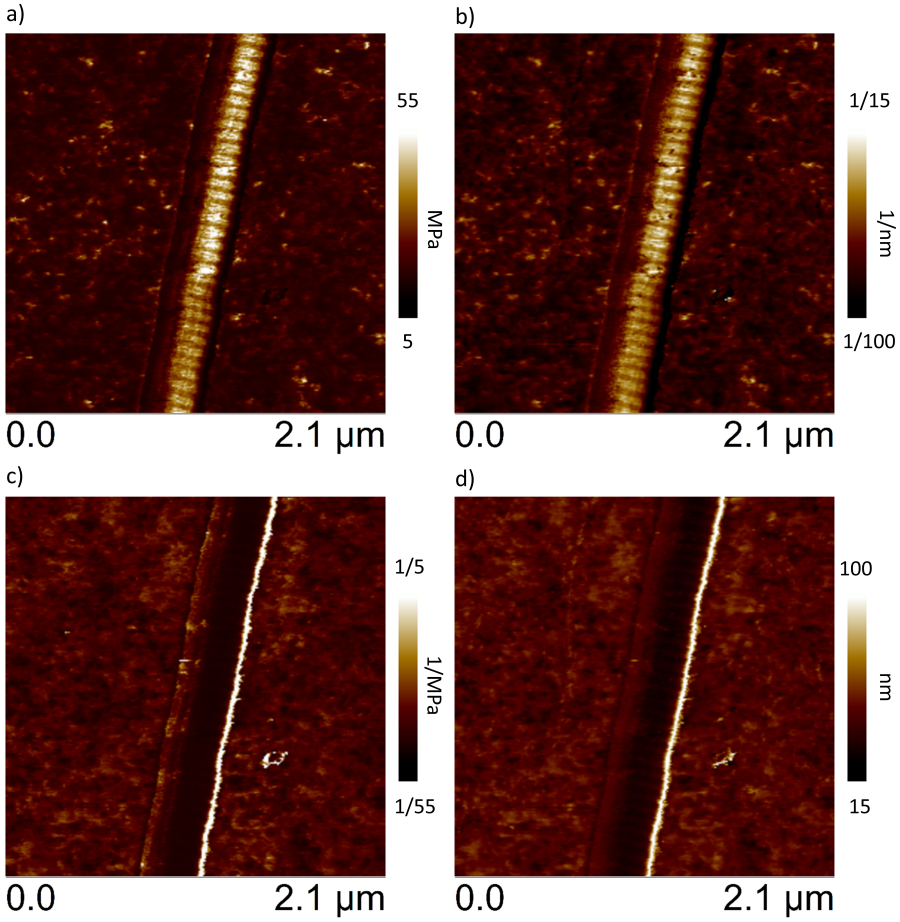

Figure 2.6: *Modulus and deformation images (a) and d)), compared to images composed of their inverse pixel values (b) and c). Alignment of (modulus, inverse deformation) and (deformation, inverse modulus) images in rows allows for the comparison and contrast between each pair of images. Note that although the inverse modulus,deformation images are qualitatively similar to the deformation, modulus images (ie. ab and cd), there are subtle differences such as a lower relative contrast in the inverse deformation image along the collagen fibril, compared to the higher contrast in the modulus image. The colour map for the pairs of images were chosen such that contrast between regions in the substrate region of the image were comparable to one another.)*

measurements [73]. The sum of these two images was then plane leveled and height measurements were obtained from the resulting image (known as the *zero force height* image). However, this operation assumes not only that the cantilever deflection is consistent throughout the image (which is only true if the peak force error remains close to zero), but also that the substrate beneath the collagen fibril being indented is not deformed by the cantilever. For this particular experiment however, the high

topographic variation and elastically compliant PDMS substrate fails both assumptions.

As opposed to simply adding the height and deformation images to generate a zero-force-height image, in this study the height was corrected by the relative average deformation measured on the fibril and the substrate. h, the measured height, is related to the undeformed (or 'true') height h_0 through the difference between fibril deformation d_f and substrate deformation d_s (figure 2.7). This was done using the following process: a line-wise level was applied to the raw height image to set the substrate height in the image to 0. Fibril height profiles were extracted from this leveled image as lines running along the apex of the fibril. The average value of the fibril deformation profile d_f was added to h and the substrate deformation d_s (average from all pixels in the image, excluding a $1\mu\text{m}\times2\mu\text{m}$ region centered on the fibril) was subtracted from average height plus average deformation value to obtain the *average substrate corrected zero force height* value h_0. All heights reported in this study are corrected using this procedure; this *average substrate corrected zero force height* is referred to simply as *height* for the remainder of this thesis.

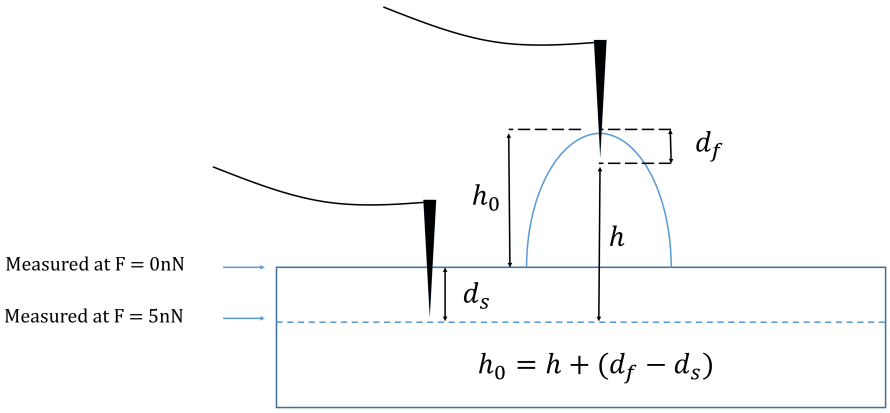

Figure 2.7: *Fibril height measurements are corrected by the difference in deformation of the fibril and the deformation of the PDMS substrate. This correction is made with the assumption that deformation measured on the apex of the fibril is entirely fibril deformation, rather than a combination of fibril and substrate deformation.*

2.6.5 Profile Extraction

From each 2μm$\times 2\mu$m image, an averaged linear profile (between 1μm and 2μm in length) was drawn along the apex of the fibril in the region of interest. With an $2\mu m \times 2\mu m$ image resolution of 256, 7 parallel lines centered around the highest point on the fibril were averaged to obtain a 60nm width-averaged profile. The position and orientation of this profile was copied across the height, deformation and indentation modulus images of the same region. A profile from each of these images was extracted and saved, from which mean values and standard deviations were calculated. The D-band and stiffness modulation of the collagen fibril was extracted by further applying Fourier analysis to the modulus profile (see section 2.6.6 for details).

2.6.6 D-band length

In order to extract the average D-band length and gap-overlap stiffness contrast from the indentation modulus profiles, any long-range variation in fibril stiffness that is not associated with the D-band must be filtered from the profile. To do this, a high-pass filter is applied to the profiles by subtracting a 30-pixel local average modulus from the profile. The width of the local averaging window is equivalent to a distance of 230nm along the fibril apex, or slightly more than three D-band periods. This width was chosen so that the filter is assured to include at least three D-band periods in the averaging even after the fibril has been strained by as much as 15%. To determine D-band length, the high-pass filtered profile was Fourier transformed and the peak of the frequency spectrum between $10\mu m^{-1}$ and $20\mu m^{-1}$ (representing D-band lengths between 50nm and 100nm) was determined using Matlab. This frequency peak was then inverted and interpreted as average D-band length for the profile. To extract the local variation in fibril stiffness, the root mean squared value of the D-band modulus oscillation was recorded from the high-pass filtered profile. This value was interpreted as the variation in fibrillar density between the gap region of the fibril's D-period and the overlap region, as per Baldwin's interpretation of the indentation modulus contrast [73]. Using this interpretation, the gap/overlap modulus ratio was then calculated from the local modulus variation using equation 2.2.

$$G/O = \frac{\langle E \rangle - \sqrt{\langle (E - \langle E \rangle)^2 \rangle}}{\langle E \rangle + \sqrt{\langle (E - \langle E \rangle)^2 \rangle}} \tag{2.2}$$

2.6.7 Statistics

Mentions of significance when comparing two distributions of data in this report refer to the use of a 2-sample paired Student's t-test. These tests were performed using the *ttest* function in Matlab. For this test, the null hypothesis was rejected for acceptance probabilities less than 5%. When linear regression was performed, the fit statistics were obtained by performing an ANOVA test on the fit line paired with the data. The linear regression and following ANOVA statistics were obtained using the *fitlm* and *anova* functions in Matlab.

Chapter 3

Results

3.1 Overview

A total of 8 individual fibrils were strained and analyzed, all sourced from the same Common Digital Extensor tendon. These fibrils were investigated at a biologically relevant salt concentration (1× PBS). A maximum extension of 30% strain was applied to the PDMS strip, after which the strip would be de-strained as the motors return to their original positions. Five of the 8 fibrils were incrementally strained to 30% and were subsequently returned to their original length. The remaining three fibrils de-laminated from the PDMS at an intermediate strain increment before the maximum strain could be reached, and in these cases the experiment was halted at the strain increment where the de-lamination occurred. Each of the 8 samples had 3 images taken of adjacent regions along the middle of the fibril, for the purposes of having a 5-6μm region from which to extract modulus, deformation and height measurements.

3.2 Initial state of collagen fibrils

An average measurement for each of the observables described in section 2.6 was obtained from the 24 images captured at 0% strain (8 fibrils, 3 regions of interest per fibril), to compare to values measured at subsequent increments of strain (see table 3.1). Average measurements for modulus and deformation compare favorably with those made on CDE tendon collagen fibrils by Quigley et al. [23]. Furthermore, measurements of height (209 ± 26nm), deformation (63 ± 27nm), modulus (12 ± 9MPa), Gap/overlap ratio (0.85 ± 0.04) and D-band length (67 ± 2nm) made in this study are quite closely related to the properties of collagen fibrils obtained from rat tail tendon, extracted by Baldwin et al. [73]. D-band length and Gap/overlap modulus ratio measurements are consistent both between tissue types as well as with

the classical Hodges-Petruska molecular packing model [17], demonstrating that the gap-overlap modulus ratio effectively captures the density contrast between the two regions.

Table 3.1: Initial conditions for 5 data-types: height, D-band length, deformation, modulus and gap/overlap modulus ratio. Included with these averages is the number of images used for each calculation; this number was less than 24 (8 samples × 3 regions per sample) because there were 8 images where the D-band could not be measured reliably.

Data type	Average ± SD	Number of images
Height (nm)	213 ± 24	24
D-band length (nm)	67 ± 2	16
Deformation (nm)	63 ± 27	24
Modulus (MPa)	7.1 ± 4.4	24
Gap/overlap modulus ratio	0.85 ± 0.04	16

3.3 Collagen fibrils under tension

3.3.1 Fibril length and structure under strain

When subjected to applied strain, the majority of measured fiducial strains were found to be less than the strain applied by the clamp motors (figure 3.1a). This is in line with the calibration results, where the strain on the distance between like hexagon vertices was observed to be consistently smaller than the substrate strain by several percent (see figure 2.2). Note that not all of the individual fiducial strain-applied strain curves are monotonic; this suggests that some fibrils experienced loss of adhesion with the substrate, partially de-laminating from the PDMS surface and slipping as strain was applied. In the instances where fibrils remained adhered to the substrate for the maximum 30% applied strain and subsequent de-straining, the fiducial length was observed to decrease when the substrate was returned to 0% strain. However, the magnitude of this decrease was found to be inconsistent between fibrils. This indicates that the loss of adhesion between the fibrils and the substrate was sporadic throughout the straining process, and unique for each fibril imaged.

The D-band length was also observed to increase with applied strain. At the first increment of applied strain (5%), the D-band was observed to strain by 4.4±6.7% (figure 3.1b), with strain values for individual fibrils reaching more than 10%. This

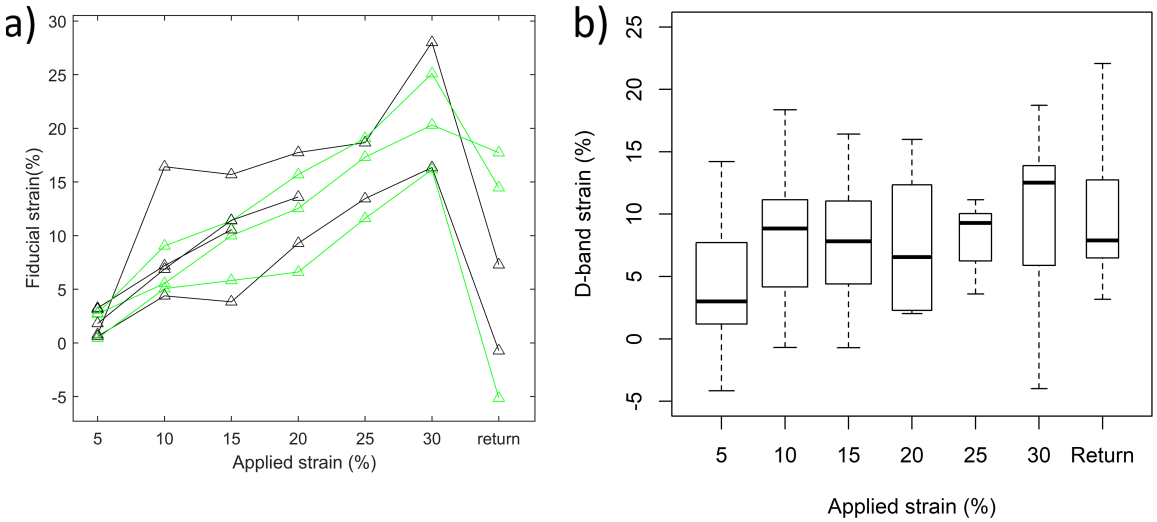

Figure 3.1: *a) Fiducial strain versus applied strain for all samples prepared in this investigation, the two colors were introduced to improve clarity. Measuring the fiducial strain from an image of a fibril introduces a pixel size error of* $\pm 0.5 - 1\%$. *b) D-band strain versus applied strain averaged over all samples. The thick black bar represents the average value, the box represents the first quartile of the set, the dotted bars represent the range of data. The D-band was found to be significantly larger than the unstrained values for all subsequent strain increments (paired Student's T-test,* $p \leq 0.05$*).*

magnitude of D-band strain is greater by a factor of two than D-band strain measurements obtained through X-ray scattering experiments [59] [42]. As was the case with the fiducial strain (figure 3.1a), the change in D-band strain with applied strain is inconsistent between fibrils. This variability speaks to the uncontrolled local, microscopic strain not directly following the macroscopic applied strain. Furthermore, the D-band strain on average tends to fall short of the applied strain (9.9±12.3% D-band strain at 30% applied strain). The magnitude of this average lag in strain is greater than the lag observed in the PDMS calibration in figure 2.2, and is therefore likely a product of the sporadic fibril de-lamination. Unexpectedly, all D-band strain measured after the PDMS was returned to 0% strain were found to be positive, and on the order of the D-band strain value measured at 30% applied strain (figure 3.1b). This is evidence that the fibril experienced relatively uniform plastic deformation at the molecular level.

The height of the fibrils was not significantly affected by the application of strain to the PDMS substrate. The fibril height was found to change by less than 15% of their

original height throughout all applications of strain. Furthermore, the changes in height that did occur were inconsistent in direction both between fibrils and between applied strain increments on the same fibril (figure 3.2a). However, when the PDMS was returned to its original unstrained length, a majority of the fibrils swelled by more than 15% of their initial height (figure 3.2b).

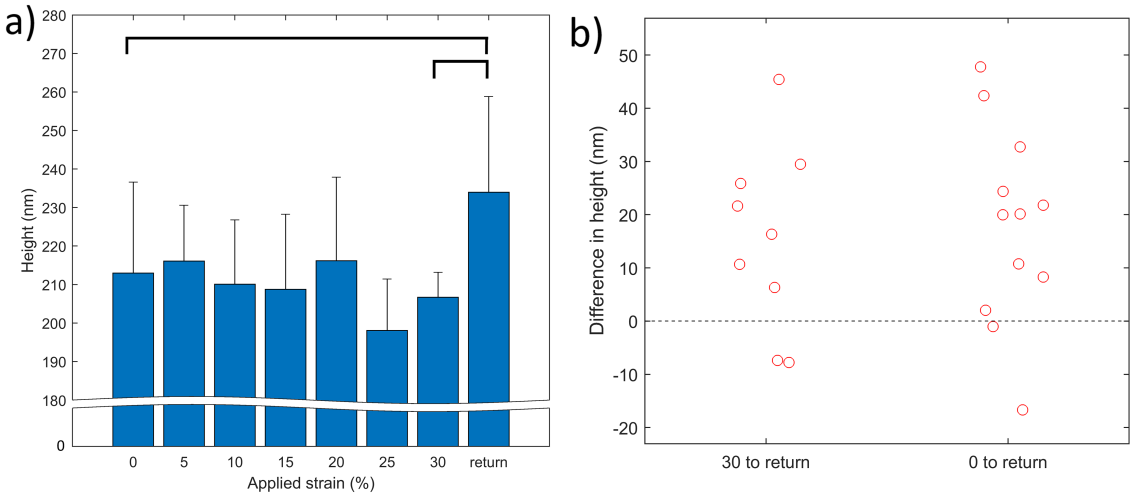

Figure 3.2: *a) Height as a function of applied strain, averaged over all regions measured. Brackets indicate significant change in height within the same region when comparing 0% and 30% strain with the return (paired Student's t-test, $p \leq 0.05$). b) Average height difference measured for each region when comparing 0% and 30% strain with the return, only significant differences are included (paired Student's t-test, $p \leq 0.05$). Swelling occurs upon return in at least 80% of the measured regions in both cases.*

3.3.2 Lateral stiffening of PDMS substrate under strain

A distribution of PDMS modulus values was extracted from each image by excluding a region containing the fibril that was $1\mu m$-wide and as long as the fibril in the image (see figure 3.3a for an illustration of this exclusion area). Due to the log-normal shape of this distribution (figure 3.3b) we avoided using the arithmetic mean as an average measure of PDMS modulus, and instead simply report the mode modulus value of the distribution.

The applied deformation to fibrils in this study was, in cases, larger than 50μm. Considering that the fibril height was consistently close to 200nm in all experiments,

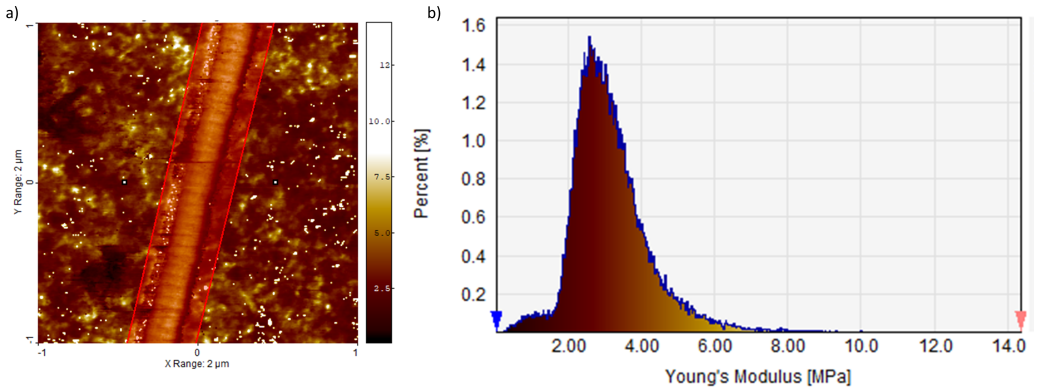

Figure 3.3: *In this figure, a) illustrates the area of excluded pixels around the fibrils, to be ignored when generating a b) distribution of PDMS modulus values.*

this magnitude of deformation (≈30% the fibril height) exheeds the 10% limit introduced by Bueckle [80]. To demonstrate that the indentation modulus of the substrate did not affect measured fibril modulus values (due to the substrate bottom effect), Figure 3.4a is a plot of the ratio between mode PDMS modulus and fibril average modulus. Notice that the ratios of the PDMS/fibril modulus values for all images are found within the range of 0.1→1 (figure 3.4b), and that the median value of this ratio tends to decrease with applied strain. This demonstrates that the stiffness of fibril and the PDMS both depend on strain but that the PDMS does not control the observed fibril stiffening.

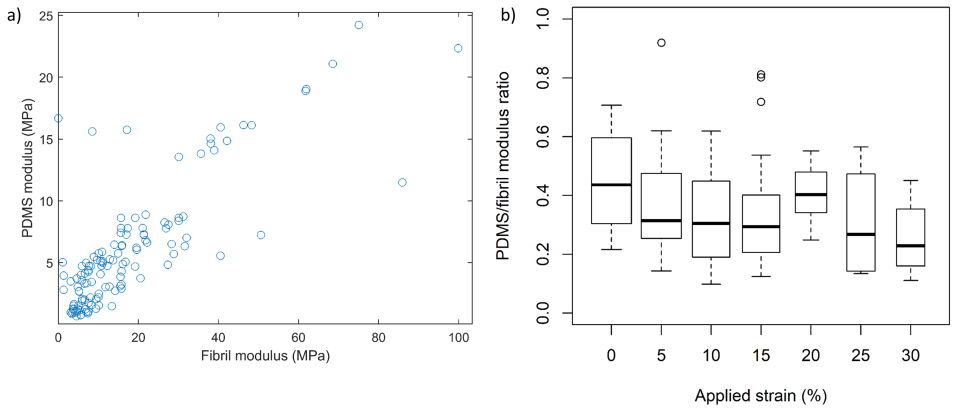

Figure 3.4: *a) PDMS modulus measurement versus the respective average fibril modulus measurements. The ratio of PDMS/fibril modulus, as a function of applied strain. The thick black bar represents the median value, the box represents the first quartile of the set, the dotted bars represent the range of data.*

Using a similar process the PDMS deformation values were extracted from each image, and the arithmetic average of each distribution was compared to the respective average fibril deformation value. Here, the arithmetic average was chosen to represent the average PDMS deformation because the distribution of these values were found to be normal in shape (not shown here), in contrast with the log-normally distributed PDMS modulus values. Figure 3.5a demonstrates that these quantities trend linearly when compared on a between fibrils, however by comparing the histograms of the ratio of average PDMS deformation and average fibril deformation ($\gamma = \frac{deformation_{fibril}}{deformation_{PDMS}}$) generated for each applied strain increment, we notice that the peak of the distribution shifts to lower γ values at larger applied strain (3.5b). This further demonstrates that mechanical measurements made on fibrils are not entirely controlled by the mechanics of the substrate to which they are adsorbed.

The radial stiffness of a bulk elastic material has in the past been treated as a proxy for axial stress [81]. By applying this interpretation here, the indentation modulus can be plotted as a function of D-band strain to represent an approximate stress-strain curve (figure 3.6). However, this treatment assumes that the material being stretched is entirely elastic, as the previous stress history of the fibril leading to each measurement in the stress-strain scatter-plot is not accounted for. D-band strain measurements have demonstrated that fibrils experience irreversible D-band lengthening at some point in the straining procedure (figure 3.1). Once this plastic deformation has occurred, releasing tension from the fibril will not result in a proportional change in the D-band length. Therefore the D-band length is not causally related to the indentation modulus, as the relationship between the two quantities is complicated by the stress history of the collagen fibril. This interpretation explains some of the spread in measured modulus values with D-band strain.

3.3.3 Radial stiffness of fibrils under strain

The adsorbed fibrils were observed to stiffen when strain was applied to the substrate, as indicated by an increase in the indentation modulus measured on the fibril between 0% and 5%, 30% strains (Figure 3.7 b and c). There is an inverse relationship between indentation modulus and deformation as discussed in section 2.6.2, and so the brightening of the fibril in the modulus images with strain (figure 3.7c) is paired

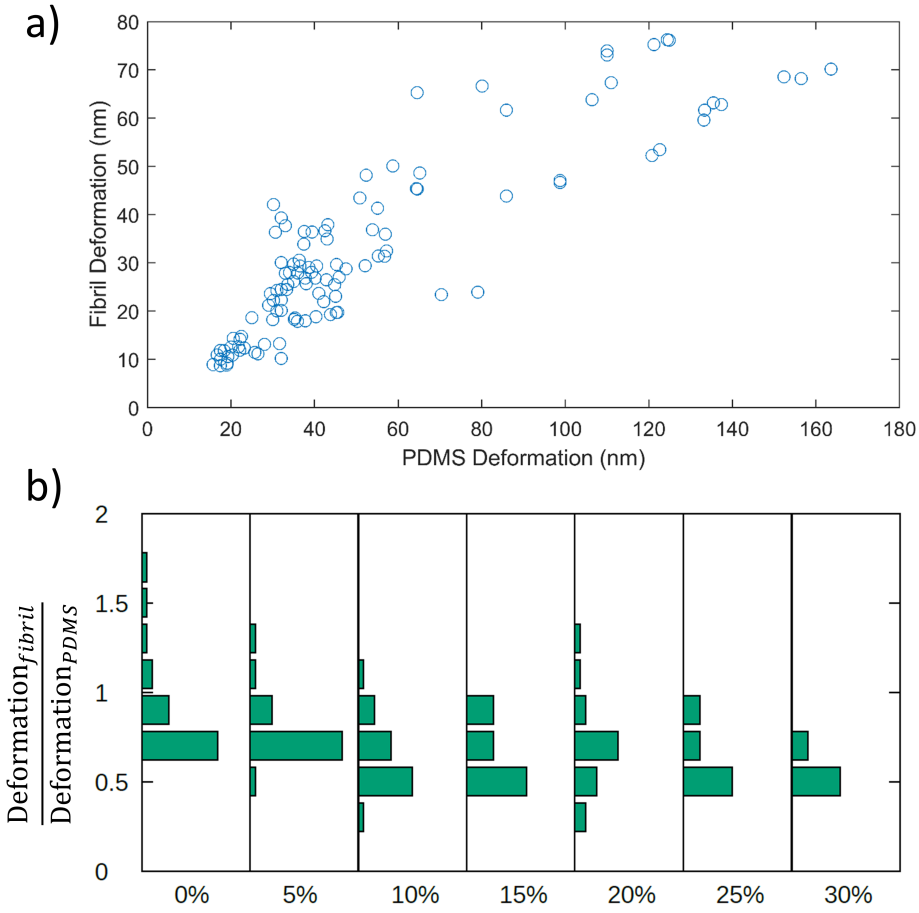

Figure 3.5: *a) A plot of PDMS deformation versus fibril deformation, for all images obtained in this experiment. b) For each increment of applied strain, a horizontally-aligned histogram presenting the distribution of fibril-PDMS deformation ratios.*

with a darkening of the fibril in the deformation images (figure 3.7b). The most significant and consistent change in fibril stiffness occurs when first increment of strain is applied (5%), where the average indentation modulus is observed to more than double (∼7MPa to 20MPa, figure 3.8). This change was paired with a halving of the deformation (from 60nm to 35nm on average, figure 3.8b). However, all subsequent applications of strain had little effect on the stiffness of fibrils with the exception of the return to 0% from maximum strain, where all fibrils were observed to soften from their respective measurements made at 30% applied strain (figure 3.8c,d).

Qualitatively, the D-band striation pattern became more visible in the modulus images as strain was applied to the fibrils. This indicates that the stiffness contrast

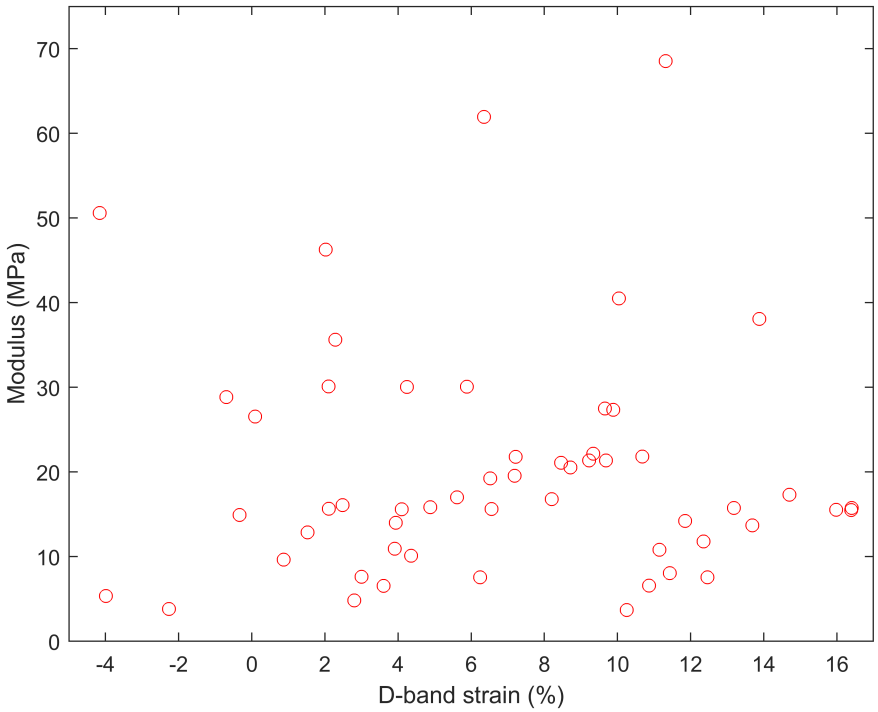

Figure 3.6: *Profile-averaged modulus plotted as a function of D-band strain, for all images captured from 0% to 30% applied strain. With the assumption that indentation modulus can be taken as a proxy for applied axial stress, this plot could be interpreted as a stress-strain curve and compared to results from Quigley et al. (figure 1.2), with the caveat that increasing D-band measurements were not made consecutively in time.*

between the gap and overlap regions becomes larger when the fibrils are extended, or at the very least when the fibrils are held in tension. This effect can be seen by comparing the unstrained and 30% applied strain log(modulus) images in figures 3.7c,d. To quantify this increase in contrast, the gap/overlap modulus ratio was calculated in proxy with equation 2.2, where the average gap modulus is estimated with the average profile modulus minus the root mean squared variation in the modulus, and the overlap is taken to be the average modulus plus the root mean squared variation. This gap/overlap ratio is observed to decrease significantly between the initial measured value and subsequent measurements at 15%, 20% and 30% applied strain (see figure 3.9).

However as demonstrated in figure 3.1, the D-band strain does not monotonically follow the strain applied to the PDMS by the motors. To avoid convolving the effect of

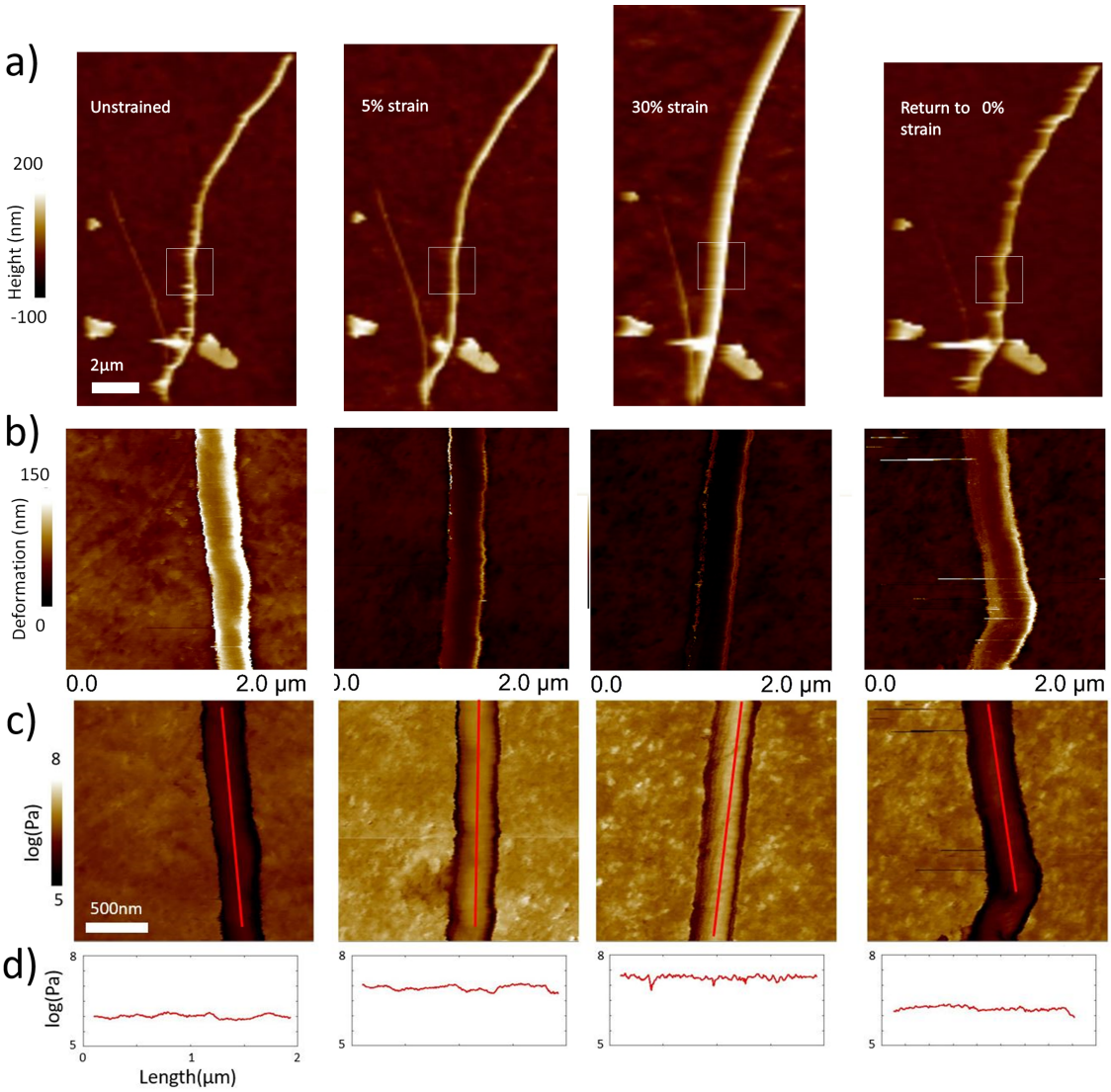

Figure 3.7: *a) Four large scale, low resolution height images of a collagen fibril at 0%, 5%, 30% strain and return, respectively; the white box represents the region in which the high resolution image was captured. b) Four high-resolution deformation images corresponding to the regions outlined in white in the first row. c) Four high-resolution log-modulus images corresponding to the regions outlined in white in a). d) Profiles extracted from the high resolution log-modulus images, corresponding to the red line drawn at the apex of the fibril in each image. Note the increase in average modulus with applied strain, and the drop in modulus upon return from maximum extension. In addition the modulus fluctuation associated with the D-band increases with applied strain, compare 0 and 30% strain.*

strain on the Gap-overlap modulus ratio with the inconsistent relationship between D-band length and applied strain, this ratio is plotted versus fibril D-band strain (figure 3.10). By comparing fibril-to-fibril changes in this way, the relationship between these

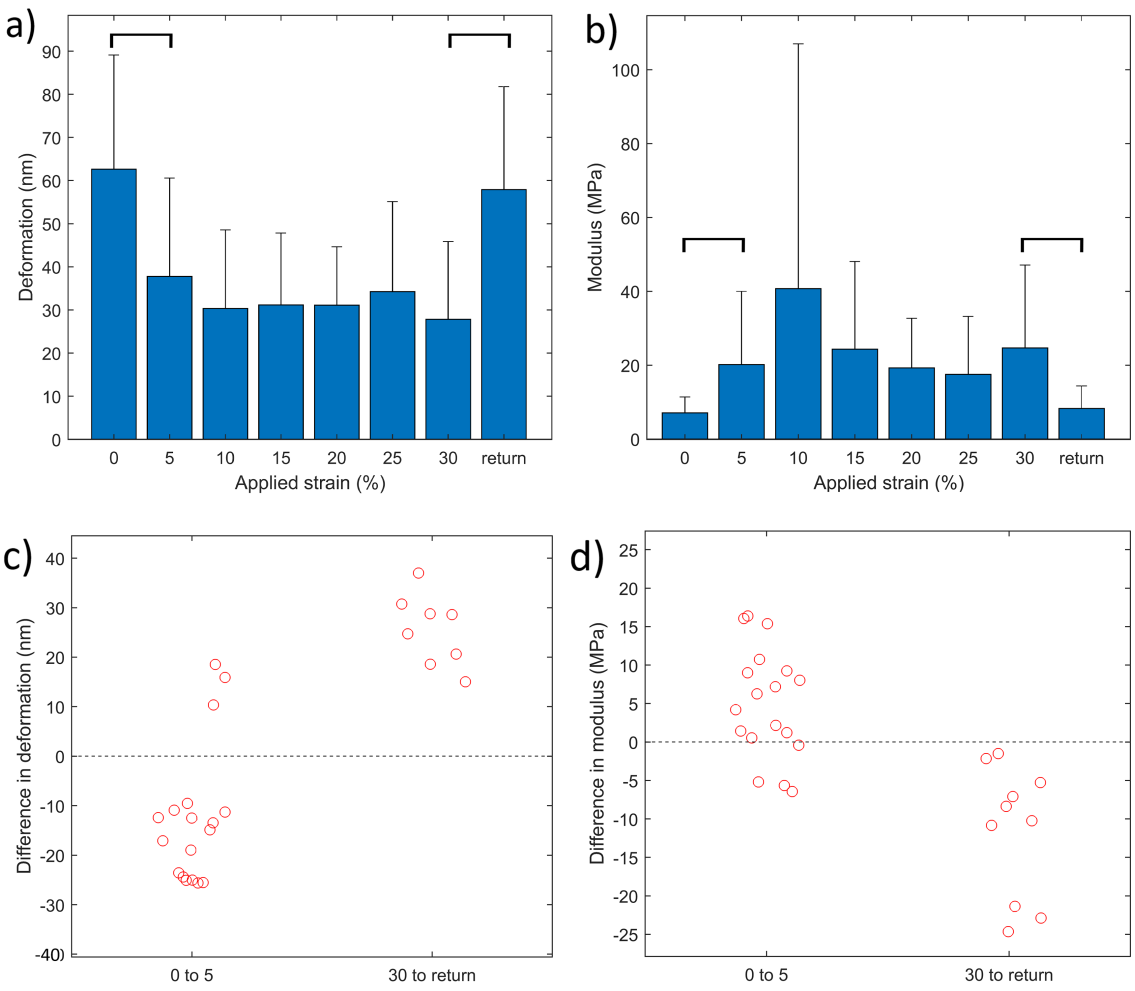

Figure 3.8: *a) Deformation as a function of applied strain, averaged over all regions. Brackets indicate significant change in deformation within the same region when comparing 0% with 5% strain and when comparing 30% strain with the return (paired Student's t-test, $p \leq 0.05$). b) Modulus as a function of applied strain, averaged over all regions. Brackets indicate significant change in modulus within the same region when comparing 0% with 5% strain and when comparing 30% strain with the return (paired Student's t-test, $p \leq 0.05$). c) Average deformation difference measured for each region when comparing 0% with 5% strain and when comparing 30% strain with the return, only significant differences are included (paired Student's t-test, $p \leq 0.05$). d) Average modulus difference measured for each region when comparing 0% with 5% strain and when comparing 30% strain with the return,only significant differences are included (paired Student's t-test, $p \leq 0.05$, as indicated by the horizontal square bracket).*

two quantities becomes strikingly linear. Note that this treatment assumes that the change in gap-overlap modulus contrast is explicitly driven by the strain in the D-band (or that whatever is driving the D-band to increase is similarly altering the

modulus contrast). Furthermore, this plot assumes that there is no hysteresis in the modulus contrast with D-band strain, so that a fibril with a 5% D-band strain at 10% applied strain will have the same structural characteristics as a fibril with 5% D-band strain at 30% applied strain.

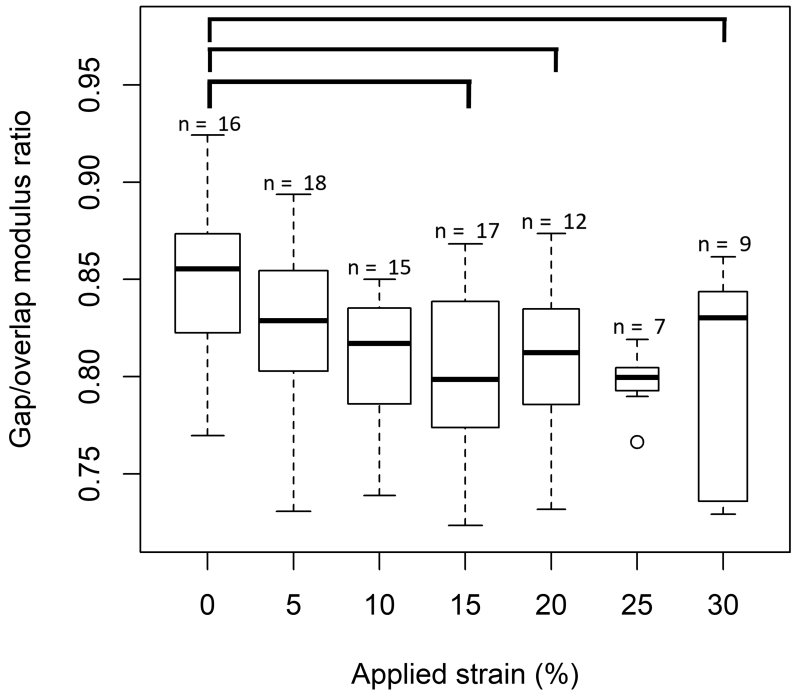

Figure 3.9: *Gap/overlap modulus ratio versus applied strain. The thick black bar represents the average value, the box represents the first quartile of the set, the dotted bars represent the range of data. The gap/overlap modulus ratio was found to decrease significantly compared to the initial values for the 15%, 20% and 30% strain increments (paired Student's t-test, $p \leq 0.05$).*

3.4 High-resolution nanomechanical mapping

In an effort to strengthen the claim that the gap and overlap regions experience different amounts of strain when the fibril is held in tension, a series of high-resolution nanomechanical maps were captured on a collagen fibril at several increments of applied strain. Following the sample preparation procedure outlined in section 2.2 collagen fibrils were dissected from a common digital extensor tendon, and were adsorbed to a PDMS film before being dried overnight. Note that the common digital extensor tendon used in the preparation of this sample was a separate specimen from

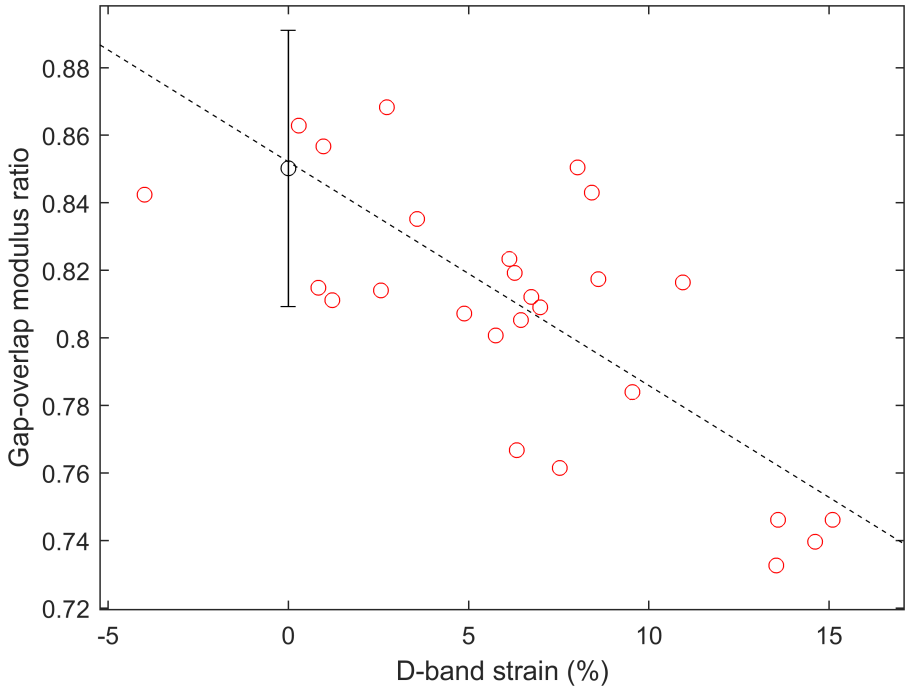

Figure 3.10: *Gap/overlap modulus ratio versus D-band strain. Each red data point represents the 3-region average values of gap/overlap and D-band strain. The open black circle with error bars represents the average value and standard deviation for the G/O before strain is applied. The linear fit was calculated by excluding the unstrained values and was found to be significant with* $R^2 = 0.54$ *and a p value of* $p = 2.15 \times 10^{-5}$.

the one used in the report, however the tissue was sourced from the same local slaughterhouse (Oulton farm, Nova Scotia, Canada) as before. The incremental straining experiment was repeated using the same protocol used in section 2.5.2, however the resolution of the nanomechanical maps was increased to ∼2nm/pixel, by capturing 500nm × 500nm images at 256 pixels/side . In addition, for the purposes of reducing the pressure applied by the tip to the sample when scanning at such high resolution, the peak force setpoint was reduced to 1nN, but otherwise all other parameters of the scan were kept to values outlined in the manuscript (a tip velocity of 1.2mm/s, a peak force frequency of 1kHz, a peak force amplitude of 300nm, and a scan rate of 0.5Hz).

Four high-resolution nanomechanical maps were acquired, one each at 0, 5, 10 and 15% applied strains (figure 3.11). Profiles were drawn along the apex of the fibril, using a similar procedure to what was used in the $2\mu m \times 2\mu m$ images, with

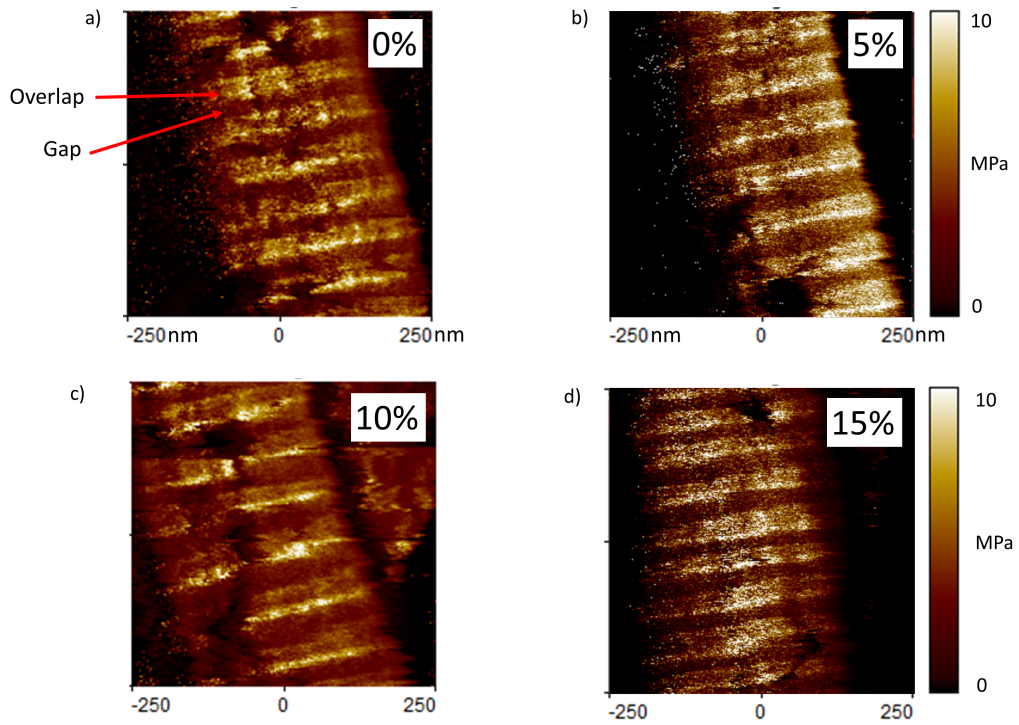

Figure 3.11: *500nm×500nm nanomechanical maps of a collagen fibril at 0,5,10 and 15% applied strain (a,b,c,d respectively). The solid blue line represents the profile that was drawn along the apex of the fibril, and the dotted lines represent the extent of adjacent lines that were averaged in the extracted profile.*

the exception that 99 adjacent lines were average over here rather than the 7 used before. Similar to what has been observed in previous experiments, the D-band strain did not follow the substrate strain. The range of modulus values between the gap and overlap, normalized by the average modulus value of the extracted profile, was found to increase from the 0% image to the 30% image. This is in agreement with the observed decrease in gap/overlap ration with D-band strain presented earlier (figure 3.10). In addition, the finer features in the overlap region were noticed to evolve in character as a function of strain (figure 3.11 a $\rightarrow$ b,c; there is an increased contrast in stiffness between the two thin 'bands' making up the overlap). An interpretation of these results is presented in the discussion section.

Chapter 4

Discussion

4.1 The relative merits of past and present Methodologies

As stated in the introduction section, the collagen fibril straining method introduced in this thesis is a successor to an experiment originally performed by Wenger et al. ([75]). In their experiment, dehydrated collagen fibrils adsorbed to a polymer film were subjected to 50% applied strain, after which the sample was left overnight to allow the substrate to creep and dry before imaging. Topographs of the fibrils were obtained using an AFM operating in tapping mode. Their goal was to quantify the difference in Poisson ratio between the gap and overlap regions of collagen fibrils by measuring the change in relative height between the two regions before and after strain was applied. This relative height (what they refer to as the *D-banding height*) was found to decrease linearly with D-band strain, thus demonstrating that there is a mechanical contrast between the two regions.

However, this approach to investigating the mechanical variation along the length of a collagen fibril has several disadvantages to the method outlined in this thesis (hereon referred to as the *hydrated QNM straining*, or the *current* method). Firstly, in order to capture the D-band height variation along the fibrils, the imaging was done in air using a contact AFM imaging mode. Not only is the dry fibril system not as biologically relevant as the hydrated system, the process of drying the fibril post-strain introduces structural changes to the fibril and its constituent triple-helixes, complicating the interpretation of morphological changes with strain [36]. Secondly the hydrated QNM straining method measures directly mechanical changes at the D-band level of the fibril with strain, whereas the technique introduced by Wenger measures only structural changes, and uses these as proxy to the mechanical differences between the gap and overlap regions. Although the method performed by Wenger and coworkers has the advantage of measuring structural changes of many

fibril in parallel on the same strained sample, the current method provides the capability of recognizing changes within the same 6μm length of fibril at many increments of applied strain. In doing so, local mechanical information is obtained on individual fibrils as a function of strain.

A disadvantage of the hydrated QNM straining procedure is the time required to investigate the mechanical properties of a single fibril as a function of strain. In order to achieve the high spacial resolution required to resolve the D-banding striation (<10nm/pixel), the nanomechanical maps were limited to be $2\mu m$ in size (because images captured using the Peakforce QNM imaging mode have a maximum resolution of 256 $\times$ 256). Therefore, investigating just a $6\mu m$ length of fibril at 7 increments of applied strain requires 21 images, each image requiring $\sim$9 minutes to capture using the imaging parameters outlined in the materials and methods section. Combined with the time required to find the fibril in the optical microscope after every increment of strain, to capture a large-scale topograph, to strain the fibril and to exchange the PBS imaging medium, strain data for a single fibril requires a full day of imaging. There is therefore a significant contrast in throughput between the current method and the straining method introduced by Wenger. In addition, the current method requires the investigator to removing and reattaching the glass clamp several times during the experiment, as well as exchange the PBS solution between strain increments. This extra sample contact-time adds to the delicate nature of the experiment, as well as the complexity of interpreting the results obtained using this method.

Quigley and coworkers were the first to demonstrate a change of stiffness and diameter of single collagen fibrils, using their bowstring stretching methodology [23]. This method has the advantage of allowing both the applied stress and the post-strain radial modulus to be measured on the same fibril. However, because an AFM cantilever is used to control the strain applied to the fibril, measuring the radial modulus as a function of applied strain is impossible. Furthermore, this method inherits the same problems with strain localization (at the glue-points and cantilever contact point) that were experienced by van der Rijt et al. in their nanofishing experiment [61]. This localization of stress affects the uncertainty in true stress applied to the fibril during extension, however it does not affect the local mechanical/structural

changes induced in sections of the fibril far from the glue/cantilever contact points. By adsorbing the entire fibril to the PDMS, stress localization at any one axial position along the collagen fibril ceases to be an issue for the hydrated QNM straining method. However, relying on the transmission of strain from the PDMS to the fibril reduces the amount of control this method has over either stress or strain applied to the fibril. In addition, the time required to strain the PDMS, re-attach the glass clamp and re-engage the AFM cantilever makes capturing the strain-relaxation behaviour of the collagen fibril impossible, considering that the fibril relaxation time has been estimated to be on the order of 1-2 minutes [82]. What the hydrated straining method lacks in mechanical control over the fibril, it gains by maintaining the stability of the fibril's strained state for subsequent imaging.

There are several ways in which the hydrated straining method could be improved. Firstly, the PDMS could be treated to increase the strength of the fibril's adhesion to the film surface (such as with a rotating plasma jet [83] or patterning the film's surface with micro-channels [84]). This treatment would reduce the risk of fibril delamination during the application of applied strain, and would likely improve the linearity of the applied strain/D-band strain relationship. Alternatively, individual fibrils could be glued at both ends to the PDMS surface using a micro-manipulator coated in epoxy [23], which would assure fibril adhesion to the surface with the drawback of introducing sites of stress-localization at the glue points. To better match the PDMS modulus to the fibril modulus (and thereby improve uniform straining on the PDMS surface near the fibril), PDMS films could be manufactured in-house with an extended curing time/increased curing temperature to increase the film stiffness [85]. Increasing the stiffness of the PDMS would also decrease the oscillations excited in the suspended film when engaged by an AFM with no glass support, thus removing the requirement for a cover slip held beneath the sample while capturing images. This simple change to the experimental procedure would decrease the time between applied strain increments and decrease the amount of contact that the investigator has to make with the sample.

4.2 Strain-induced structural changes

One of the common methods used to measure the mechanical response of fibrils under strain is through X-ray scattering performed on strained tissue [57] [58] [59] [60] [86]; this technique was pioneered by Mosler et al. [87], and experiments based on their methodology have been performed as recently as 2 years ago [42]. Scattering intensity profiles obtained from Small Angle X-ray Scattering (SAXS) measurements contain information pertaining to periodic structures within the tissue [57]. These profiles can be obtained in real time during the tissue-level tensile test (>1 profile/second) and, by fitting the scattering results in reciprocal space to a real-space scattering model, provide a movie of how the fibrillar structure changes with applied load. A consistent observation made in these scattering experiments is a substantial decrease in strained fibril diameter, coupled with an increase in D-band length. This gives the impression of a large fibrillar Poisson ratio, which is surprisingly not evident from the experiments performed in the current study (figure 3.2). This discrepancy in observation is likely a product of the differences in methodology between the two studies; adsorbing the collagen fibrils to the surface of a deformable substrate likely affects the capability of the fibrils to contract laterally when subjected to axial straining. If the fibril remains perfectly adsorbed to the substrate throughout the straining process, then the contraction of the adsorbed surface of the fibril will be dictated by a combination of the mechanical properties of both the bulk PDMS and that of the PDMS-fibril interface.

An observation that is consistent between various X-ray scattering studies is that the actual D-band strain measured from the scattering profiles are consistently smaller than the applied tissue-level strain. This is seen in the current study as a lag between applied strain and fiducial strain, as well as between applied strain and D-band strain. The strain applied to the PDMS film was found to exceed the measured fiducial and D-band strains at most strain increments, for a majority of the samples prepared (figures 3.1). Few D-band strain measurements exceeded 20%, and only one measurement was greater than 30% (the 10% applied strain measurement from the high-resolution trial, see section 4.5). Clearly the D-band strain does not follow the applied strain monotonically; this is likely due to slippage occurring between the substrate and the fibril. Although the mechanism by which the strain-lag in the PDMS-fibril system

is by no means the same mechanism controlling the tissue-fibril strain lag, it is clear in both systems that inhomogenous microscopic strain follows applied macroscopic strain.

In a SAXS-based tissue-level experiment performed by Wells et al., strain applied to a section of bovine pericardium resulted in an observed increase in D-band length, which was paired with a decrease in fibril diameter [58]. The D-band length was determined from the 9th-order diffraction peak of the integrated intensity plots, and the average fibril diameter was measured by fitting the SAXS intensity plot obtained at an angle perpendicular to the average fibrillar long axis to a model based on a cylindrical form-factor. However, in this study the largest average D-band strain obtained from tissue straining was $\sim$4.5%, with a corresponding change in fibrillar diameter on the order of $\sim$10%. A change in fibril height is observed in the current study that has a range of 10-15% the unstrained value. However as discussed previously in this section, this height change is inconsistent not only between fibrils, but also between strain increments and does not occur in exclusively one direction. The difference in approach here is that in the current study, height is measured directly as the difference in height between the fibril apex and the substrate, and is corrected by the average deformation made both to the fibril and to the PDMS. Wells et al.'s method has the advantage that measurements of fibril diameter are not convolved with the changes in substrate roughness with strain or by changes in the fibril's adhesion to the substrate, both of which likely affect the change in fibril diameter when strain is applied. In addition, the X-ray scattering method provides a multi-million fibril average measurement of diameter, whereas the current method is restricted to an average measurement over a $\sim 6\mu m$ length on a single fibril. As for the D-band strain, I observe values in excess of 3$\times$ the values obtained by Wells et al. for individual fibrils, although the average strain over all fibrils tested in this study remains close to 5%.

4.3 Post-strain morphological changes

In the last decade, there has been a progressing development in methods used to strain and subsequently evaluate the structural properties of individual fibrils. In their single-fibril bowstring stretching study, Quigley et al. pre-conditioned their

fibrils by strain-cycling them once by 3-4% before performing further tensile tests [23]. They noticed a significant swelling of the pre-conditioned fibrils by more than 30% of their original height on average (figure 4.1, first row). Similarly in the current study a majority of the fibrils were observed to swell when the PDMS is returned from 30% applied strain, although the magnitude of the post-strain swelling observed here was half that of the observations from Quigley et al. (15-17% on average). To compare the results from the current study to those obtained by Quigley, the change in height before and after fibril straining is compared to the maximum strain achieved by the fibril in extension. We find that only 6 images of all those taken in this study contained fibrils that were successfully strained to 30% and had a corresponding D-band measurement at 30% applied strain. From these data, the average *swelling ratio* ($Height_{return}/Height_{initial}$) was 1.18 ± 0.12 (n = 6), with an average D-band strain of $9.9 \pm 8.0\%$ (n = 6). The height ratio here is above 1 in all cases, and the most substantial swelling (swelling ratio ≈ 1.4) was achieved at a D-band strain of $\sim$10%.

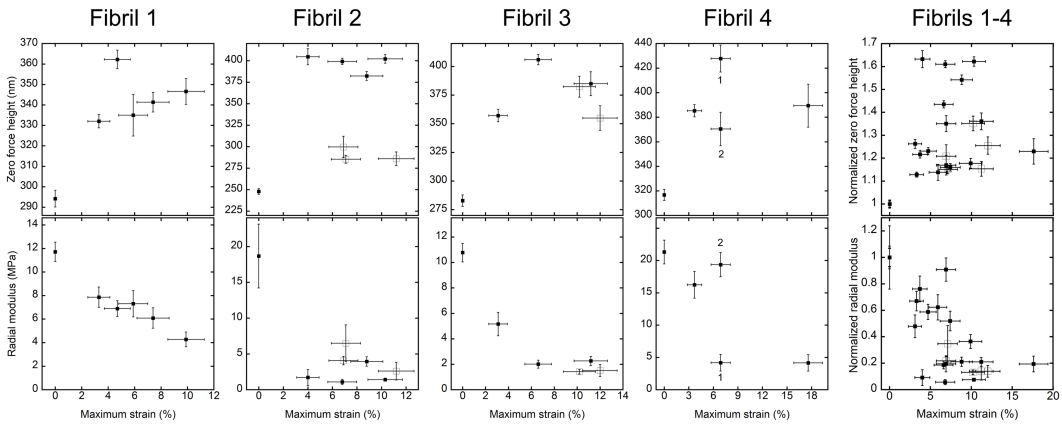

Figure 4.1: *Height and indentation modulus vs. maximum strain achieved during tensile testing for each fibril segment in Quigley et al.'s bowstring stretching study. The first datapoint above 0% strain are the pre-strain only measurements. The two panels at the far right are plots of* normalized *fibril height and modulus (analogous to swelling and stiffening ratios described here, respectively) versus maximum fibrillar strain obtained via tensile testing, for all fibrils tested in this study. Figure reprinted from [23], figure 3*

For Quigley et al., all fibrils were found to swell between their unstrained state and their state after pre-conditioning, however only a subset of the preconditioned segments underwent further swelling at subsequent applications of strain (figure 4.1).

In addition, fibrillar swelling after pre-contioning was paired in all cases with a radial softening of the fibril. To compare to these findings, the average *stiffening ratio* ($Modulus_{return}/Modulus_{initial}$) was calculated from all images where the D-band strain could be measured at 30% applied strain and found to be 0.75 ± 0.44 (n = 6). This, paired with the observed average D-band strain of 9.9 ± 8.0 at 30% applied strain demonstrates that the most likely response of a fibril that experiences D-band strain is to soften upon return. This agrees well with the previously stated observations made by Quigley et al. (figure 4.1) [23]. Note that the low number of data points in these average ratio calculations is in part due to the low number of samples that were successfully strained to 30% and returned, and also in part due to the limited number of images where the D-band frequency signal could be reliably measured from the profiles.

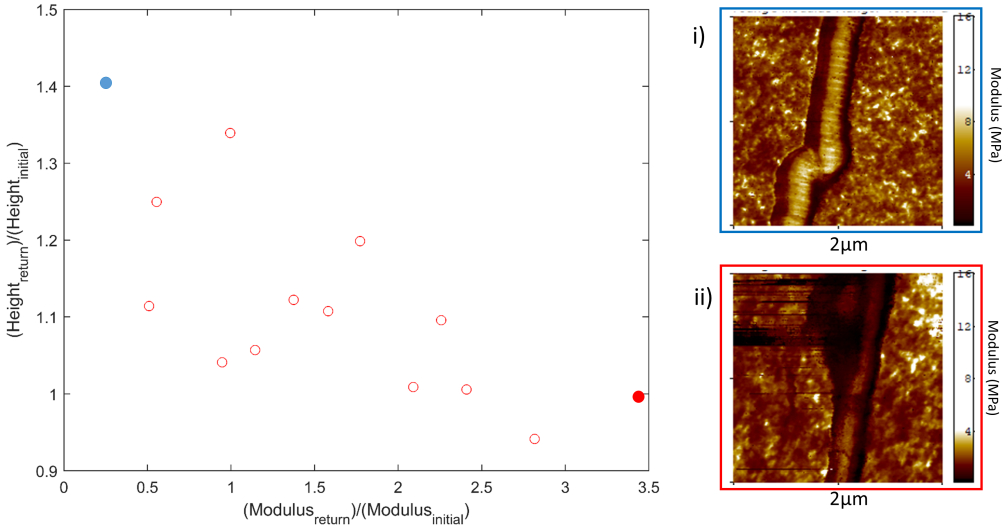

Figure 4.2: *Ratio of height measured on return to height measured before strain application, versus the ratio of modulus measured on return to modulus measured before strain application. i) Nanomechanical map of fibril returned from maximum extension, corresponding to the lowest final/initial modulus ratio (blue filled point). ii) Nanomechanical map of fibril returned from maximum extension, corresponding to the highest final/initial modulus ratio (red filled point).*

The previously mentioned average stiffening/swelling ratios were calculated using only modulus/height ratios that had corresponding D-band strain measurement at 30% applied strain. This was done for a more direct comparison to Quigley et al.'s results, since in their study they were able to measure fibrillar strain and

swelling/stiffening ratios for all strained fibril sections. By removing the requirement that the D-band strain was measurable at 30% applied strain, a larger number of stiffening and swelling ratios can be reported from the current study (going from n=6 to n=14 measurements for each quantity). Interestingly, the swelling ratio appears to be negatively proportional to the stiffening ratio when the two are plotted against each other (figure 4.2), where the largest swelling occurred for fibrils that also softened after being strain-cycled. This downward trend is consistent with Quigley et al.'s suggestion that the uptake of water into the fibrillar structure (swelling) has the effect of softening the fibril substantially [23]. More surprisingly, a large number of fibrils were found with a stiffening ratio greater than 1 and a swelling ratio close to 1 (between 0.9 and 1.2), which were previously omitted from the stiffening ratio average (for their lack of D-band strain measurement). This suggests that there is a population of fibrils that have low radial stiffness contrast which respond to being strain-cycled by stiffening, while maintaining a similar diameter to what they had before strain was applied. The observation that a majority of fibrils (n = 9 out of 14 total) stiffened after straining is inconsistent with Quigley et al.'s observations; this is likely due to the difference in strain application methodologies between the two studies.

In addition to swelling, fibrils that were strained to 30% and returned to 0% applied strain all experience what appears to be compression buckling (figure 4.3). Compression buckling occurs only if the fibril was in a relaxed state when the PDMS was at 30% strain, so that when the PDMS is released from stress the fibril becomes stressed again, now in compression. There are two ways in which the fibrillar structure could relax while lying on a stressed PDMS substrate: Firstly, if the fibril has extended plastically as a result of applied strain; secondly, if the fibril has slipped from its original position on the PDMS at some point throughout the extension experiment, keeping its original (or close to original) length as the substrate is strained.

The shape of these buckles varies widely from fibril to fibril, however here I will introduce the two more common morphologies observed on return. The first behavior is what I will refer to as *shear dislocation*, a buckling morphology that is observed in hollow cylindrical rods (such as straws and carbon nanotubes [88]) where a section of

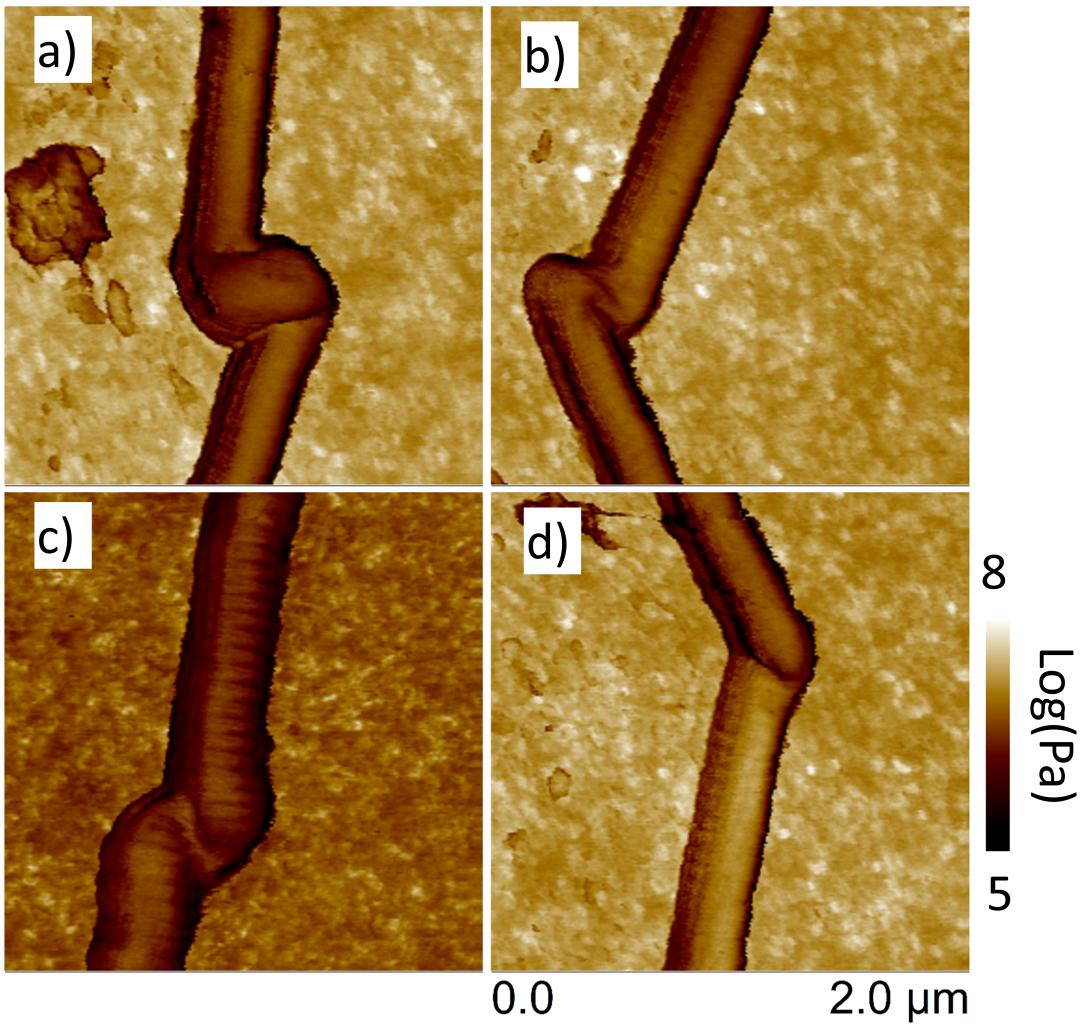

Figure 4.3: *Four examples of localized fibril buckling, occurring upon return to zero strain from maximum applied strain. The morphology of this buckling varies both between fibrils as well as between regions on the same fibril.*

the rod displaces laterally at a point along its axis with the region between the two dislocated sections experiencing plastic damage. Figure 4.3b in particular demonstrates fibrillar buckling that resembles shear dislocation. In figure 4.3a and c, the fibrils appear not to have developed a simple point dislocation, but rather have undergone a complete twist around their axis and folded over themselves at the buckling site. This second behavior I refer to as *end-overs*; a buckling morphology reminiscent of torsional instability in compressed twisted ropes [89]. These observations further

support the notion that fibrils are intrinsically twisted structures, with compression buckling morphology similar to that experienced by macroscopic wire cables [90].

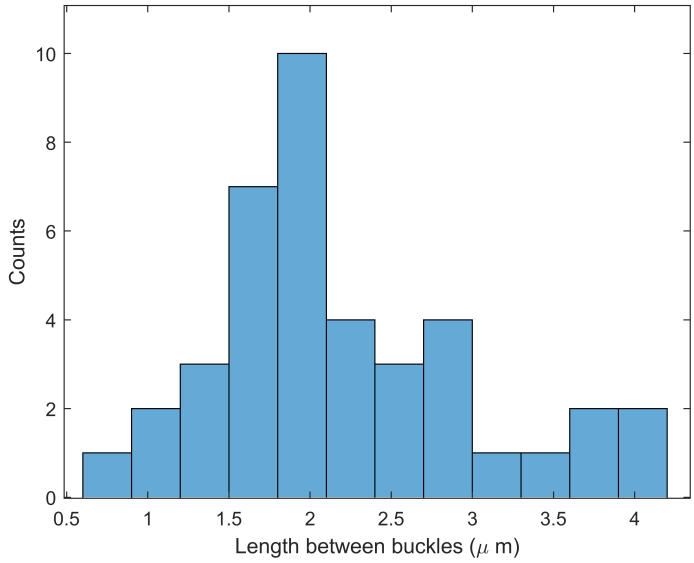

Figure 4.4: *A histogram of the length measured between adjacent buckling sites, on fibrils that were strained to 30% applied strain and returned to 0% applied strain. All buckle-to-buckle distances were measured from the low-resolution 50μm images, with an estimated uncertainty of 0.1μm for each measurement.*

In addition to having relatively consistent morphology between fibrils, the buckling occurred with a regular period of 2μm (see figure 4.4), with a range in individual measurements between 1 and 4μm. This suggests either that magnitude of fibril compression is consistent throughout the extension experiments, or that there exists periodic mechanical weak points along the fibril with a length-scale on the order of 1-4μms.

4.4 The average indentation modulus as a readout of fibril tension

The indentation modulus of the fibrils is observed to effectively double after the first 5% increment of strain is applied to the PDMS substrate (figure 3.8b,d). However after this first increment of strain, no significant change in indentation modulus occurs for any subsequent application of strain. This behaviour is consistent with the idea that the molecules within the fibrillar structure are being tauted in this first strain increment, and that any subsequent application of strain is simply working to

maintain this molecular tension [91] [35] [92]. Keeping with this interpretation, the increase in D-band length with applied strain occurs while the molecules composing the collagen fibril remain taut and under tension. However the lack of a significant trend between the D-band length and the modulus demonstrates that whatever mechanism is driving the D-band strain to increase is separate from the mechanism that causes an increase in indentation modulus. If molecular tauting is truly responsible for the increase in fibril stiffness, then the indentation modulus would be expected to return to the original unstrained value when the fibril is returned from extension (ie, the molecular tension causing the tauting is removed). This is observed as fibrillar softening on return, with the indentation modulus decreasing from maximum extension (30%) to return (figure 3.8d). At the same time, the D-band is observed to remain significantly longer than the measurements made before applying strain. This observation is further evidence that some other deformation mechanism is contributing to D-band strain, so the tauting of molecules within the structure is not solely responsible for this lengthening.

Analysis of the fibrillar modulus has never been performed as a function of strain, so no direct literature comparison can be made to the measurements made in this study. However, the indentation modulus of isoprene rubber has been measured as a function of applied strain, with the classically expected result that increased extension of the rubber leads to an increase in measured indentation modulus [81]. This is due to strain reducing the entropic lateral motion of polymer chains in the bulk material, making the rubber more energetically-costly to extend with lateral indentation. A similar observation is made in the current study; a majority of the fibrils increase in modulus with the first increment of applied strain, however for all subsequent strain increments the change in indentation modulus becomes inconsistent between both separate fibrils and between regions on the same fibril. This demonstrates that collagen fibrils behave similarly to a much more extensible bulk rubber for applied strains less than $\sim$5%, but that another (plastic) deformation mechanism takes over the structural evolution of the fibril beyond this point.

Baldwin et al., in their pioneering work on nanomechanical measurements made on hydrated collagen fibrils [73], recognized that the modulus ratio of the gap and overlap regions of the fibril was, within statistical uncertainty, the same as the theoretical

density ratio proposed in the Hodges-Petruska molecular stacking model [17]. In addition to repeating this observation for unstrained fibrils on PDMS, we also observe a significant decrease of this ratio with fibrillar strain. Thus far, there have been no claims for how the mechanical contrast (or molecular density, as the mechanical contrast is a proxy for) should change with fibrillar strain. Therefore this observation is a novel one in the collagen fibril literature. These observations are discussed in further detail in the next section 4.5.

4.5 Collagen fibrils have an axially inhomogeneous response to applied tension

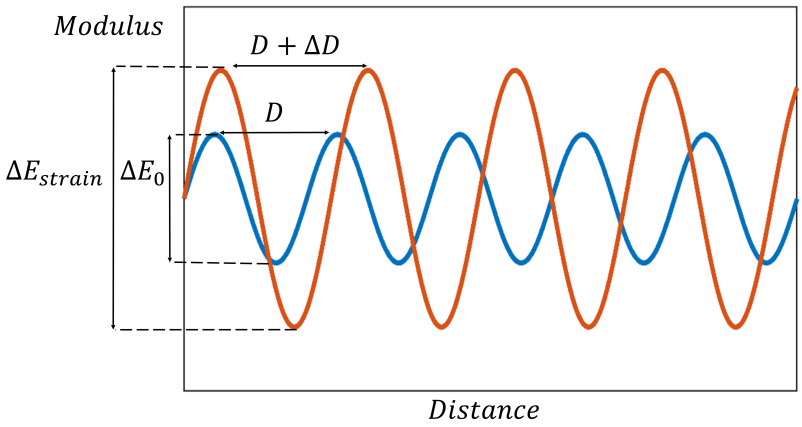

Figure 4.5: *An illustration of the increase in gap/overlap modulus contrast with D-band strain.*

The gap/overlap modulus ratio of the collagen fibril has been observed to decrease with both fiducial strain and D-band strain (Figures 3.9 and 3.10). The gap region of the D-band appears about 15% less stiff under indentation than the overlap region in a fibril's unstrained state (Figure 3.10); this contrast nearly doubles to 25% when the D-band is extended by 20% of its original length (illustrated in figure 4.5). Using Baldwin et al.'s interpretation that the indentation modulus is proportional to molecular density, an increase in regional contrast speaks to a reorganization of the fibrillar structure at the D-band level, and therefore the molecular level [73]. This reorganization likely occurs through a combination of plastic and elastic mechanisms as the D-band is observed to both increase and subsequently decrease at later strain

increments (figure 4.6b), as well as remain at a strained D-band length even when the PDMS is returned to its unstrained length after extension (figure 4.6a).

One hypothetical model for how this structural change occurs with strain is that molecules in the gap region experience a larger magnitude of strain than those in the overlap. By increasing the length of the gap region with respect to the overlap and maintaining the lateral dimensions of both regions, the gap region becomes sparser than the overlap with strain. This is in agreement with SAXS-based studies, which consistently observe that the gap experiences more strain than the overlap when tissue is extended [35] [92].

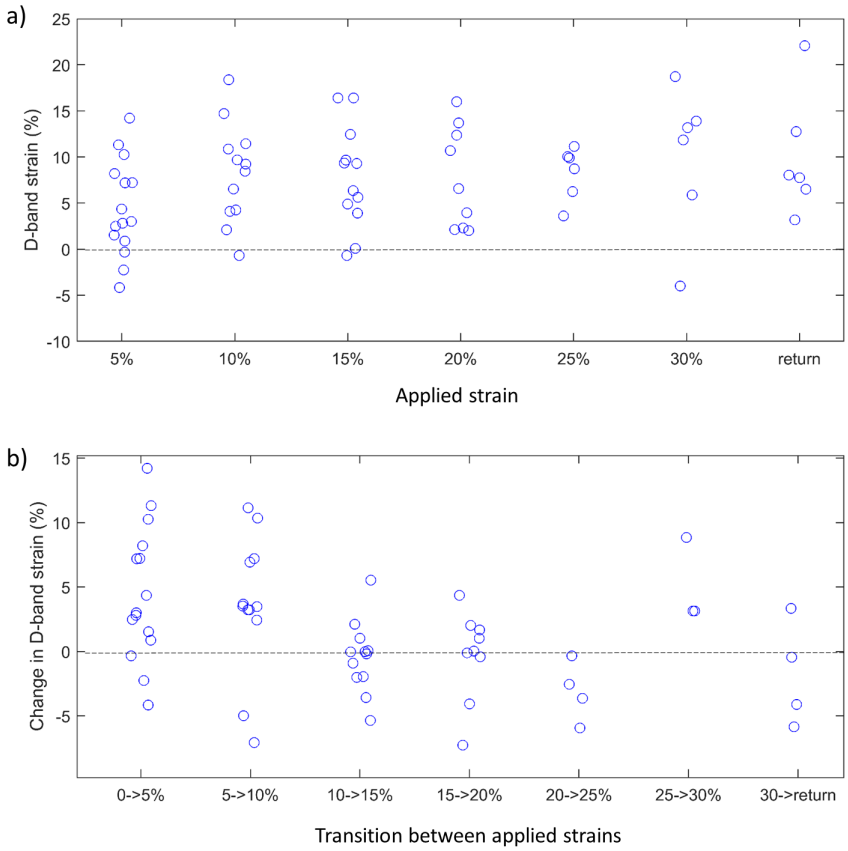

Figure 4.6: *a) A scatter-plot of D-band strain values, as a function of applied strain. b) A scatter-plot of the changes in D-band strain values between increments of applied strain. Notice that in the first two applications of strain ($0 \rightarrow 5\%$ and $5 \rightarrow 10\%$), the D-band is more likely to increase, however for all subsequent applications of strain the D-band is no more likely to increase than it is to decrease with applied strain.*

It is likely that the differential stiffening of the gap and overlap regions is a product of a change in relative hydration between the two regions. Rarefaction of collagen within the gap region may cause a net influx of water, now capable of filling the gaps between the taut molecules. This would happen to a lesser degree (or not at all) within the overlap region; the difference in water influx would further contrast the mechanics of the two regions. Interestingly, the increase in regional modulus contrast is not associated with an increase in average fibrillar modulus (figure 3.6), demonstrating that these two observables are likely controlled by distinct deformation mechanisms.

Results from the high-resolution nanomechanical mapping experiment illustrate in detail the axially- inhomogenous response of the fibril to strain. The goal of this experiment was to confirm that the gap region extends proportionally more than the overlap region. However, the finer features in what was initially referred to as the overlap region were noticed to evolve in character as a function of strain (figure 4.7a,b; there is an increased contrast in stiffness between the two thin 'bands' making up the initial overlap region). This evolution in structure makes it difficult to definitively pick out the start and end points of the gap and overlap regions, and so the absolute length of the gap and overlap regions became impossible to measure objectively. As an alternative to using subjective features of the D-band striation pattern to measure the gap and overlap lengths, a horizontal line was plotted through the modulus profile average, and the area between the regions above and below this line were compared before and after strain (figure 4.7c,d). Using this approach, the proportional difference in length of the gap and overlap regions (i.e., the relative areas above and below the average line) can be seen to change when the fibril is strained. Without repeating this experiment several more times for many increments of applied strain, these images will remain the limit of detail in this discussion of how the fibrillar structure evolves with strain.

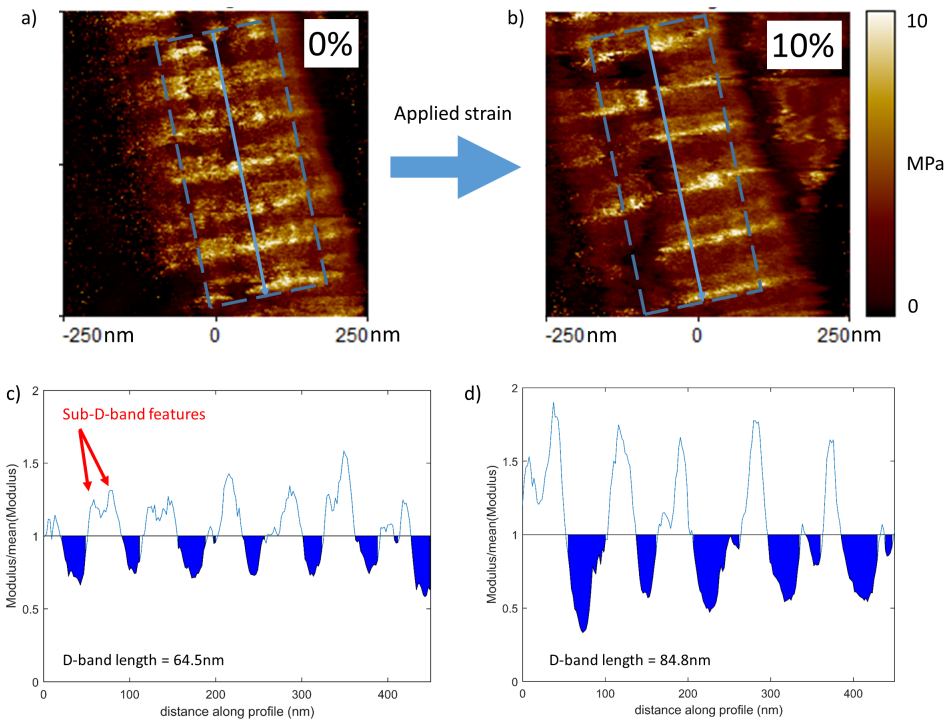

Figure 4.7: *500nm×500nm nanomechanical maps of a collagen fibril a) unstrained and b) in a strained state (10% applied strain). c) and d) are 99-line averaged profiles drawn along the apex of the fibril in it's unstrained and strained states, respectively. To demonstrate that the gap and overlap regions are changing in length a line was plotted through the average modulus value of each profile, and the area between the average-normalized profile and the straight line running through the average was filled.*

In addition to an increase in the contrast in modulus mentioned in the results section, these high-resolution images suggest a modulus contrasting develops between sections of the overlap region within a D-band repeat. These periodic features of finer detail have been observed in cryo-EM images (see figure 4.7c) [93], and are attributed to an increased molecular density due to the axially contracted telopeptide domains of the collage molecule's N- and C-termini. The presence of these bands in the nanomechanical maps obtained in the current study once again demonstrates that indentation modulus can be used as an effective proxy to molecular density. Interestingly, the collagen molecule C- and N- termini are also suggested in previous works to be sites of inter-molecular covalent cross-linking within the fibrillar structure [93]. If this change in mechanical contrast is taken to represent a change in molecular density, then these results demonstrate that the telopeptide domains of the collagen

molecule's termini are being extended by differing amounts when strain is applied to the fibril. Alternatively, if changes in indentation modulus are interpreted as changes in molecular tension, then the increase in modulus contrast between the edge-regions of the overlap is evidence that the termini are being subjected to different magnitudes of tension when the fibrillar structure is tensed. However, due to the preliminary nature of these few results, a future investigation will be required to make a more definitive statement of how the sub-D-band structure is changing with applied strain.

4.6 Molecular unfolding and sliding within the gap region

Considering that common digital extensor tendon fibrils have been observed to mechanically yield in extension at ∼5-10% strain in a previous tensile studies [29], it is conceivable that D-band strains that exceed 5% in the present study represent the development of fibrillar plastic damage. Plastic damage would explain the remnants of D-band strain and gap-overlap modulus ratio decrease after the fibril has been maximally strained and returned; particularly, the irreversible change in mechanical contrast speaks to a re-distribution of material between sections of the fibril. A likely mechanism by which this re-distribution occurs is the sliding of adjacent molecules within the fibrillar structure, as has been suggested to occur at ∼15% fibrillar strain in Depalle et al.'s 2016 molecular dynamics simulation [76]. The strain rate in this MD study was however 10 orders of magnitude higher than the strain rate used in the current study, and so the molecular sliding likely occurs at fibrillar strains lower than 15% in reality.

There is also evidence that the molecules themselves are accumulating damage or conformational changes, in the observation that the fibril swells significantly when the fibril is returned from maximum extension. Zitnay et al's steered molecular dynamics simulations demonstrate that uncoiling a collagen triple helix (such as the plastic damage achieved through strain) increases its capacity to form bonds with water molecules [94]. These two likely deformation mechanisms combined alter the structure and therefore the functionality of the collagen fibril, both as a microscopic strain mediator and it's capacity to bind with ligands in tissue.

Chapter 5

Conclusion

5.1 Summary of results

There are four major conclusions that can be drawn from the this study. Firstly, in agreement with previous collagen straining experiments [75] [42] [58] [59], the length of the collagen fibril D-band increases with strain applied to the fibril. Observations made after one full extensive strain-cycle suggest that at least a portion of this D-band strain is irreversible, so therefore the act of straining a fibril D-band by 5-20% permanently alters the fibril structure. Secondly, the radial stiffness of collagen fibrils increases with applied axial strain. This demonstrates that molecules within the fibrillar structure become taut when the fibril is pulled, which is evident by the reversal of the radial stiffening when tension is released from the fibril. Thirdly and unexpectedly, this radial strain-stiffening of the collagen fibril is inhomogeneous along the length of the fibril; molecular tautening is concentrated in the gap region where the molecular density is low with respect to the overlap region. Fourthly, we find that this change in stiffness contrast is dependent on the magnitude of D-band strain applied to the fibril, so just as the D-band strain is partially irreversible, so too is the structural change associated with the increase in indentation modulus contrast. Lastly, there is an inhomogenous distribution of stress within the overlap region of the D-band. The high-resolution images obtained of a fibril under tension demonstrate that the peaks in indentation modulus associated with the C- and N- termini of the collagen monomers become more contrasted as a function of D-band strain. Coupled with the suggestion from the literature that these features are the sites of enzymatic cross-linking between adjacent molecules in the fibrillar structure suggest that the two regions are unequally loaded.

5.2 Significance

The current work set out to capture changes in collagen fibril structure as a function of applied strain. Not only was this goal achieved in the observed increase in D-band length and post-strain swelling, but also observed were two distinct mechanisms for structural reorganization that affect the indentation modulus: (1) global fibrillar stiffening through molecular tension and tautening, and (2) changes in local density contrast through inhomogeneous axial strain. This is the first study to directly observe structural-mechanical changes in collagen fibrils as a function of strain, and furthermore the first to demonstrate that changes in the mechanical properties of collagen fibrils with strain are region-specific and vary along the fibril axis.

5.3 Response to initial research questions

In the introductory section, two research questions were asked in anticipation of being answered by results obtained from the experiments performed in this thesis. The following are responses to these questions, based on my observations:

1.*Can this (D-band) strain inhomogeneity be observed directly by imaging individual fibrils at several increments of applied strain?*

While the gap and overlap lengths were not measured separately, the increase in D-band length coupled with a mechanical contrast between the two regions suggests that the unequal straining observed by Gautieri et al [42]. using SAXS also occurs on an individual fibril basis. Therefore the answer to this question is a qualitative 'yes' based on a simple molecular tautening argument, which could likely be made quantitative by performing additional high-resolution imaging experiments to more accurately measure the gap and overlap lengths as a function of strain.

2.*Is the D-band length measurable beyond 5% strain? If so, does the fibril structure deform irreversibly or fail beyond 10% D-band strain?*

The answer to the first components of this question is 'yes'; the D-band is clearly

measurable after 5% strain (in fact, with greater contrast in the modulus images when the D-band is extended). This demonstrates that the loss of signal in SAXS-based D-band strain measurements beyond this threshold is a method-specific problem and does not indicate a strain-drive transition in fibril structure. As for the second component of this question, while there is certainly evidence for plastic deformation in strained fibrils (present in the irreversible increase in gap-overlap stiffness contrast and the post-strain swelling), there is no obvious mode of deformation that can be observed from the images taken in these experiments, nor is it likely that this mode is consistent for all fibrils strained in this study. This is partially due to the lack of stress/strain control using the hydrated QNM method, but also likely due to intrinsic mechanical differences between the fibrils in this experiment; one of the most striking observations made in this study was the wide range in stiffness and strain response between fibrils extracted from the same tissue model.

5.4 Next steps

The observations made in this study have provoked a series of interesting questions, which could be followed up with many individual experiments. Here are a few examples of where this investigation could go in the future:

1. Investigate the binding properties of several biologically relevant ligands (such as Integrin, Decorin, MMP, fibronectin, etc.) by performing nanomechanical mapping using an AFM cantilever functionalized with the respective ligand. This could be initially for collagen fibrils lying on glass with no applied tension, and eventually on PDMS with several increments of applied strain. As an example of this functionionalization procedure could be done by preparing a 0.1 g/L fibronectin solution and pipetting the mixture into a 1mL micropipette tip. Using a hydraulic micromanipulator with the micropipette positioned in an alligator clamp, the solution at the end of the pipette tip could be maneuvered into contact with an AFM cantilever. Once in contact, the solution-cantilever setup should be left to rest for 5 minutes (to guarantee adhesion of suspended fibronectin to the cantilever tip), after which the tip should be removed slowly from the pipette and left to air dry for at least 5 minutes. After this

process has been performed, the tip should be coated with a thin (likely less than 50nm thick) layer of fibronectin. This functionalized cantilever can then be used to image collagen fibrils adsorbed to PDMS, using the point-and shoot capabilities of a Nanoscope Catalyst AFM to indent only on the collagen fibril in the field of view of a high-resolution micrograph (reducing the number of indentations the tip makes on the PDMS substrate).

2. Repeating high-resolution nanomechanical mapping experiment for several fibrils, to confirm that the increase in mechanical contrast between the stiff features in the overlap region is consistent through many strain experiments. This could be paired with a molecular dynamics study which incorporates C- and N- terminus cross linking, to relate molecular density/tension with observations made in the nanomechanical mapping experiment.

3. Stick-slipping and/or total de-lamination from the PDMS substrate occurred for most of the fibrils studied in this experiment. The procedure outlined in this thesis could be slightly altered by gluing the ends of the fibril of interest down to the PDMS substrate with epoxy using a hydraulic micromanipulator for epoxy application, and performing all nanomechanical mapping in a region between the two glue points. This experiment would be a hybrid of the current method and the tensile testing method performed by Quigley et al. [23]; the glue would make the fibril slipping from the PDMS far less likely, and the glue points would act as fiducial markers to be used to measure true fibril strain.

4. One characteristic that differentiates fibrils form different tissue types is the density and type of cross linking within the fibril structure. The experiment could be repeated for fibrils extracted from various tissue types (such as from bovine flexor tendon, rat-tail tendon or human achilles tendon), to determine whether the fibril's structural response to tension is model-specific. In addition to in-vivo model comparisons, a similar experiment could be performed on collagen fibrils assembled in-vitro in the absence of lysyl oxydase. This would provide a minimal-cross-link control for the experimental result for each fibril model tested. Preparation of these in-vitro

samples could be done by diluting 200μL of 1g/L rat tail collagen-hydrochloric acid solution with 700μL of deionized water and 100 μL 10$\times$ phosphate buffered saline and letting the solution rest in a 30°C water bath for 3 hours. After this time, the collagen triple-helices suspended in the aqueous solution will have formed thin (10-30nm) fibrils which can be adsorbed to a sheet of PDMS or glass by depositing droplets of this solution onto the substrate and following the standard drying procedure outlined for extensor tendon fibril samples in this thesis.

5. In the current study, fibrils were observed to develop compression buckles at local sites along the fibril. This interesting morphological behaviour could be investigated in greater detail by performing hydrated compression tests in place of extension tests; adsorb collagen fibrils to a PDMS film that is *pre-strained* by the motorized stage, and release the tension in the substrate to effectively compress the fibrils. Multiple compression-extension cycles could be performed to determine whether these buckled sites nucleate fibrillar plastic damage at subsequent strain cycles.

6. Collagen fibrils are known to behave viscoelasically, where the elastic modulus in extension is dependent on extension speed. All substrate straining performed in the current study was done at a constant rate of 50μm/s (equivalent to $\sim$0.2%/s for the extension stage used here). A subsequent study could be performed in which this extension speed is varied (for instance, from 5μm/s to 500μm/s, for two full orders of magnitude of range), to qualify the strain-rate dependence of fibril mechanics. Using an AFM system imaging with a sufficiently high frame rate, the changes in fibril structure could be measured in real-time as strain is applied to the system. To minimize the effect of sample drift during imaging, the capture speed of the AFM should be such that the drift in distance over the capture time is much less than the dimensions of the image; furthermore, because the substrate would not be supported by a glass cover slide during imaging, effort would have to be made to suppress the excited oscillations of the PDMS film during imaging.

Bibliography

[1] J H Yoon. Tendon proteoglycans: biochemistry and function. *J Musculoskelet Neuronal Interact*, 5(1):22–34, 2005.

[2] Gion Fessel and Jess G Snedeker. Evidence against proteoglycan mediated collagen fibril load transmission and dynamic viscoelasticity in tendon. *Matrix biology : journal of the International Society for Matrix Biology*, 28(8):503—510, October 2009.

[3] Micheal KJÆR. Role of extracellular matrix in adaptation of tendon and skeletal muscle to mechanical loading. *Physiological Reviews*, 84(2):649–698, 2004. PMID: 15044685.

[4] J. Kastelic, A. Galeski, and E. Baer. The multicomposite structure of tendon. *Connective Tissue Research*, 6(1):11–23, 1978. PMID: 149646.

[5] K E Kadler. Collagen fibril formation. *Biochemical Journal*, 316(1):1–11, 1996.

[6] Pal Pedersen Spencer E. Szczesny, Jeffrey L. Caplan and Dawn M. Elliott. Quantification of interfibrillar shear stress in aligned soft collagenous tissues via notch tension testing. *Scientific Reports*, 5, 2015.

[7] J. Kastelic, A. Galeski, and E. Baer. The polypeptide chain configuration of collagen. *Nature*, 176:1062–1064, 1955.

[8] KA Piez and A Miller. The structure of collagen fibrils. *Journal of Supramolecular Structure*, 2:121–137, 1974.

[9] Elizabeth G. Canty and Karl E. Kadler. Procollagen trafficking, processing and fibrillogenesis. *Journal of Cell Science*, 118(7):1341–1353, 2005.

[10] Matthew D. Shoulders and Ronald T. Raines. Collagen structure and stability. *Annual Review of Biochemistry*, 78(1):929–958, 2009. PMID: 19344236.

[11] Yinhui Lu Elizabeth G. Canty-Laird and Karl E. Kadler. Stepwise proteolytic activation of type 1 procollagen to collagen within the secretory pathway of tendon fibroblasts in situ. *Biomedical Journal*, 441(2):707–717, 2012.

[12] G. N. Ramachandran and G. Kartha. Structure of collagen. *Nature*, 174(6):269–270, 1954.

[13] Darwin J. Prockop and Kari I. Kivirikko. Collagens: Molecular biology, diseases, and potentials for therapy. *Annual Review of Biochemistry*, 64(1):403–434, 1995. PMID: 7574488.

[14] Andrzej Steplewski, Hidetoshi Ito, Eileen Rucker, Raymond J. Brittingham, Tatiana Alabyeva, Milind Gandhi, Frank K. Ko, David E. Birk, Sergio A. Jimenez, and Andrzej Fertala. Position of single amino acid substitutions in the collagen triple helix determines their effect on structure of collagen fibrils. *Journal of Structural Biology*, 148(3):326 – 337, 2004.

[15] G.J. Cameron, D.E. Cairns, and T.J. Wess. The variability in type 1 collagen helical pitch is reflected in the d periodic fibrillar structure. *Journal of Molecular Biology*, 372(4):1097 – 1107, 2007.

[16] David R. Eyre, Mercedes A. Paz, and Paul M. Gallop. Cross-linking in collagen and elastin. *Annual Review of Biochemistry*, 53(1):717–748, 1984. PMID: 6148038.

[17] J A Petruska and A J Hodge. A subunit model for the tropocollagen macromolecule. *Proceedings of the National Academy of Sciences of the United States of America*, 51, 1964.

[18] John H. Lillie, Donald K. MacCallum, Lawrence J. Scaletta, and Joseph C. Occhino. Collagen structure: Evidence for a helical organization of the collagen fibril. *Journal of Ultrastructure Research*, 58(2):134 – 143, 1977.

[19] E Reale, Francesco Benazzo, and Alessandra Ruggeri. Differences in the microfibrillar arrangement of collagen fibrils. distribution and possible significance. *Journal of submicroscopic cytology*, 13(2):135–43, 1981.

[20] E.Reale A.Ruggeri, F.Benazzo. Collagen fibrils with straight and helicoidal microfibrils: a‘ freeze-fracture and thin-section study. *Journal of Ultrastructure Research*, 68(1):101 – 108, 1979.

[21] Samuel Cameron, Laurent Kreplak, and Andrew D. Rutenberg. Polymorphism of stable collagen fibrils. *Soft Matter*, 14:4772–4783, 2018.

[22] Tyler W. Herod, Neil C. Chambers, and Samuel P. Veres. Collagen fibrils in functionally distinct tendons have differing structural responses to tendon rupture and fatigue loading. *Acta Biomaterialia*, 42:296 – 307, 2016.

[23] Andrew S. Quigley, Samuel P. Veres, and Laurent Kreplak. Bowstring stretching and quantitative imaging of single collagen fibrils via atomic force microscopy. *PLOS ONE*, 11(9):1–14, 09 2016.

[24] Peter Fratzl, editor. *Collagen: Structure and Mechanics*. Springer, 233 Spring Street, New York, NY 10013, USA, 1 edition, 2008.

[25] Keith M. Meek. Corneal collagen—its role in maintaining corneal shape and transparency. *Biophysical Reviews*, 1(2):83–93, Jul 2009.

[26] John A. Trotter, Gillian Lyons-Levy, Frederick A. Thurmond, and Thomas J. Koob. Covalent composition of collagen fibrils from the dermis of the sea cucumber, cucumaria frondosa, a tissue with mutable mechanical properties. *Comparative Biochemistry and Physiology Part A: Physiology*, 112(3):463 – 478, 1995.

[27] S. Rigozzi, R. Müller, and J. G. Snedeker. Collagen fibril morphology and mechanical properties of the achilles tendon in two inbred mouse strains. *Journal of Anatomy*, 216(6):724–731, 2010.

[28] K.L Goh, J.R Meakin, R.M Aspden, and D.W.L Hukins. Influence of fibril taper on the function of collagen to reinforce extracellular matrix. *Proceedings of the Royal Society B: Biological Sciences*, 272(1575):1979–1983, 2005.

[29] Andrew Quigley, Stéphane Bancelin, Dylan Deska-Gauthier, François Légaré, Laurent Kreplak, and Samuel. Veres. In tendons, differing physiological requirements lead to functionally distinct nanostructures. *Scientific Reports*, 8, 2018.

[30] Jennifer H. Shepherd and Hazel R. C. Screen. Fatigue loading of tendon. *International Journal of Experimental Pathology*, 94(4):260–270, 2013.

[31] Kheng Lim Goh and David F. Holmes. Collagenous extracellular matrix biomaterials for tissue engineering: Lessons from the common sea urchin tissue. *International Journal of Molecular Sciences*, 18(5), 2017.

[32] Michael A. Horton Marco P. E. Wenger, Laurent Bozec and Patrick Mesquida. *Biophysical Journal*, (4).

[33] Yehe Liu, Roberto Ballarini, and Steven J. Eppell. Tension tests on mammalian collagen fibrils. *Interface Focus*, 6(1):20150080, 2016.

[34] Orestis G. Andriotis, Sylvia Desissaire, and Philipp J. Thurner. Collagen fibrils: Nature's highly tunable nonlinear springs. *ACS Nano*, 12(4):3671–3680, 2018. PMID: 29529373.

[35] Alfonso Gautieri, Simone Vesentini, Alberto Redaelli, and Markus J. Buehler. Hierarchical structure and nanomechanics of collagen microfibrils from the atomistic scale up. *Nano Letters*, 11(2):757–766, 2011. PMID: 21207932.

[36] Admir Masic, Luca Bertinetti, Roman Schuetz, Shu-Wei Chang, Till Hartmut Metzger, Markus J. Buehler, and Peter Fratzl. Osmotic pressure induced tensile forces in tendon collagen. *Nature Communications*, 6, 2015.

[37] Sheena E. Radford Colin A. Grant, David J. Brockwell and Neil H. Thomson. Tuning the elastic modulus of hydrated collagen fibrils. *Biophysical Journal*, 97(11):2985–2992, 2009.

[38] O. G. Andriotis, S. W. Chang, M. Vanleene, P. H. Howarth, D. E. Davies, S. J. Shefelbine, M. J. Buehler, and P. J. Thurner. Structure and mechanics relationships of collagen fibrils in the osteogenesis imperfecta mouse model. *Journal of The Royal Society Interface*, 12(111):20150701, 2015.

[39] Ricardo L Mancera. Does salt increase the magnitude of the hydrophobic effect? a computer simulation study. *Chemical Physics Letters*, 296:459–465, 11 1998.

[40] S R Pinnell and G R Martin. The cross-linking of collagen and elastin: enzymatic conversion of lysine in peptide linkage to alpha-aminoadipic-delta-semialdehyde (allysine) by an extract from bone. *Proceedings of the National Academy of Sciences*, 61(2):708–716, 1968.

[41] Robert C. Siegel, Roy C. Page, and George R. Martin. The relative activity of connective tissue lysyl oxidase and plasma amine oxidase on collagen and elastin substrates. *Biochimica et Biophysica Acta (BBA) - General Subjects*, 222(2):552 – 555, 1970.

[42] Alfonso Gautieri, Fabian S. Passini, Unai Silván, Manuel Guizar-Sicairos, Giulia Carimati, Piero Volpi, Matteo Moretti, Herbert Schoenhuber, Alberto Redaelli, Martin Berli, and Jess G. Snedeker. Advanced glycation end-products: Mechanics of aged collagen from molecule to tissue. *Matrix Biology*, 59:95 – 108, 2017.

[43] Yufei Li, Gion Fessel, Marios Georgiadis, and Jess G. Snedeker. Advanced glycation end-products diminish tendon collagen fiber sliding. *Matrix Biology*, 32(3):169 – 177, 2013.

[44] Gion Fessel, Yufei Li, Vincent Diederich, Manuel Guizar-Sicairos, Philipp Schneider, David R. Sell, Vincent M. Monnier, and Jess G. Snedeker. Advanced glycation end-products reduce collagen molecular sliding to affect collagen fibril damage mechanisms but not stiffness. *PLOS ONE*, 9(11):1–12, 11 2014.

[45] Rene B. Svensson, Stuart T. Smith, Patrick J. Moyer, and S. Peter Magnusson. Effects of maturation and advanced glycation on tensile mechanics of collagen fibrils from rat tail and achilles tendons. *Acta Biomaterialia*, 70:270 – 280, 2018.

[46] Zhilei Liu Shen, Harold Kahn, Roberto Ballarini, and Steven J. Eppell. Viscoelastic properties of isolated collagen fibrils. *Biophysical Journal*, 100(12):3008 – 3015, 2011.

[47] Jasper Foolen, Vikram S. Deshpande, Frans M.W. Kanters, and Frank P.T. Baaijens. The influence of matrix integrity on stress-fiber remodeling in 3d. *Biomaterials*, 33(30):7508 – 7518, 2012.

[48] Buddy D. Ratner E. Helene Sage Hua Wang, Andrzej Fertala and Shaoyi Jiang. Identifying the sparc binding sites on collagen 1 and procollagen 1 by atomic force microscopy. 77(21):6765–6771, 2005.

[49] Shiamalee Perumal, Olga Antipova, and Joseph P. R. O. Orgel. Collagen fibril architecture, domain organization, and triple-helical conformation govern its proteolysis. *Proceedings of the National Academy of Sciences*, 105(8):2824–2829, 2008.

[50] Andrew Dittmore, Jonathan Silver, Susanta K. Sarkar, Barry Marmer, Gregory I. Goldberg, and Keir C. Neuman. Internal strain drives spontaneous periodic buckling in collagen and regulates remodeling. *Proceedings of the National Academy of Sciences*, 113(30):8436–8441, 2016.

[51] J Gross and Y Nagai. Specific degradation of the collagen molecule by tadpole collagenolytic enzyme. *Proceedings of the National Academy of Sciences*, 54(4):1197–1204, 1965.

[52] J. P. R. O. Orgel, J. D. San Antonio, and O. Antipova. Molecular and structural mapping of collagen fibril interactions. *Connective Tissue Research*, 52(1):2–17, 2011. PMID: 21182410.

[53] Jie Zhu, Cody L. Hoop, David A. Case, and Jean Baum. Cryptic binding sites become accessible through surface reconstruction of the type 1 collagen fibril. *Scientific Reports*, 8, 2018.

[54] AM Cribb and JE Scott. Tendon response to tensile stress: an ultrastructural investigation of collagen:proteoglycan interactions in stressed tendon. *Journal of anatomy*, 187 (Pt 2):423—428, October 1995.

[55] Jeffrey A. Weiss Kristi A. Hansen and Jennifer K. Barton. Recruitment of tendon crimp with applied tensile strain. *Journal of Biomedical Engineering*, 124(1):72–77, 2001.

[56] Khaled M Hijazi, Kathy L Singfield, and Samuel P Veres. Ultrastructural response of tendon to excessive level or duration of tensile load supports that collagen fibrils are mechanically continuous. *Journal of the mechanical behavior of biomedical materials*, 97:30—40, May 2019.

[57] Naoki Sasaki and Shingo Odajima. Elongation mechanism of collagen fibrils and force-strain relations of tendon at each level of structural hierarchy. *Journal of Biomechanics*, 29(9):1131 – 1136, 1996.

[58] Hannah C. Wells, Katie H. Sizeland, Hanan R. Kayed, Nigel Kirby, Adrian Hawley, Stephen T. Mudie, and Richard G. Haverkamp. Poisson's ratio of collagen fibrils measured by small angle x-ray scattering of strained bovine pericardium. *Journal of Applied Physics*, 117(4):044701, 2015.

[59] Peter Fratzl, Klaus Misof, Ivo Zizak, Gert Rapp, Heinz Amenitsch, and Sigrid Bernstorff. Fibrillar structure and mechanical properties of collagen. *Journal of Structural Biology*, 122(1):119 – 122, 1998.

[60] H. R. C. Screen, J. Seto, S. Krauss, P. Boesecke, and H. S. Gupta. Extrafibrillar diffusion and intrafibrillar swelling at the nanoscale are associated with stress relaxation in the soft collagenous matrix tissue of tendons. *Soft Matter*, 7:11243–11251, 2011.

[61] Joost A. J. van der Rijt, Kees O. van der Werf, Martin L. Bennink, Pieter J. Dijkstra, and Jan Feijen. Micromechanical testing of individual collagen fibrils. *Macromolecular Bioscience*, 6(9):697–702, 2006.

[62] Barney Drake Helen G. Hansma Daniel E. Morse James B. Thompson, Johannes H. Kindt and Paul K. Hansma. Bone indentation recovery time correlates with bond reforming time. *Nature*, 414:773–776, 2001.

[63] John S. Graham, Anthony N. Vomund, Charlotte L. Phillips, and Michel Grandbois. Structural changes in human type 1 collagen fibrils investigated by force spectroscopy. *Experimental Cell Research*, 299(2):335 – 342, 2004.

[64] Thomas Gutsmann, Georg E. Fantner, Johannes H. Kindt, Manuela Venturoni, Signe Danielsen, and Paul K. Hansma. Force spectroscopy of collagen fibers to investigate their mechanical properties and structural organization. *Biophysical Journal*, 86(5):3186 – 3193, 2004.

[65] Pavel Dutov, Olga Antipova, Sameer Varma, Joseph P. R. O. Orgel, and Jay D. Schieber. Measurement of elastic modulus of collagen type 1 single fiber. *PLOS ONE*, 11(1):1–13, 01 2016.

[66] Yu-Long Sun, Zong-Ping Luo, Andrzej Fertala, and Kai-Nan An. Direct quantification of the flexibility of type 1 collagen monomer. *Biochemical and Biophysical Research Communications*, 295(2):382 – 386, 2002.

[67] Alfonso Gautieri, Monica I. Pate, Simone Vesentini, Alberto Redaelli, and Markus J. Buehler. Hydration and distance dependence of intermolecular shearing between collagen molecules in a model microfibril. *Journal of Biomechanics*, 45(12):2079 – 2083, 2012.

[68] Alfonso Gautieri, Simone Vesentini, Alberto Redaelli, and Markus J. Buehler. Viscoelastic properties of model segments of collagen molecules. *Matrix Biology*, 31(2):141 – 149, 2012.

[69] Baptiste Depalle, Andre G. Duarte, Imke A.K. Fiedler, Laurent Pujo-Menjouet, Markus J. Buehler, and Jean-Philippe Berteau. The different distribution of enzymatic collagen cross-links found in adult and children bone result in different mechanical behavior of collagen. *Bone*, 110:107 – 114, 2018.

[70] Markus J. Buehler. Nanomechanics of collagen fibrils under varying cross-link densities: Atomistic and continuum studies. *Journal of the Mechanical Behavior of Biomedical Materials*, 1(1):59 – 67, 2008.

[71] Andreas Stylianou. Atomic force microscopy for collagen-based nanobiomaterials. *Journal of Nanomaterials*, 2017:1–14, 01 2017.

[72] A review of atomic force microscopy imaging systems: application to molecular metrology and biological sciences. *Mechatronics*, 14(8):907 – 945, 2004.

[73] Samuel J Baldwin, Andrew S Quigley, Charlotte Clegg, and Laurent Kreplak. Nanomechanical mapping of hydrated rat tail tendon collagen 1 fibrils. *Biophysical journal*, 107, 2014.

[74] Robert C. Buck. Reorientation response of cells to repeated stretch and recoil of the substratum. *Experimental Cell Research*, 127(2):470 – 474, 1980.

[75] Marco P. E. Wenger and Patrick Mesquida. Longitudinal variations in the poisson's ratio of collagen fibrils. *Applied Physics Letters*, 98(16):163707, 2011.

[76] Baptiste Depalle, Zhao Qin, Sandra J. Shefelbine, and Markus J. Buehler. Influence of cross-link structure, density and mechanical properties in the mesoscale deformation mechanisms of collagen fibrils. *Journal of the Mechanical Behavior of Biomedical Materials*, 52:1 – 13, 2015. SI:Collagen mechanics.

[77] John E. Sader and James R. Friend. Note: Calibration of atomic force microscope cantilevers using only their resonant frequency and quality factor. *Review of Scientific Instruments*, 85(11):116101, 2014.

[78] Guillaume Lamour, Julius B. Kirkegaard, Hongbin Li, Tuomas Knowles, and Jörg Gsponer. Easyworm: An open-source software tool to determine the mechanical properties of worm-like chains. *Source Code for Biology and Medicine*, 9, 07 2014.

[79] Ian N. Sneddon. The relation between load and penetration in the axisymmetric boussinesq problem for a punch of arbitrary profile. *International Journal of Engineering Science*, 3(1):47 – 57, 1965.

[80] J. H. Westbrook and H. Conrad, editors. *The Science of hardness testing and its research applications.* Metals Park, Ohio : American Society for Metals, 1973.

[81] Shuquan Sun, Dong Wang, Thomas P. Russell, and Liqun Zhang. Nanomechanical mapping of a deformed elastomer: Visualizing a self-reinforcement mechanism. *ACS Macro Letters*, 5(7):839–843, 2016.

[82] Sheetal R. Inamdar, David P. Knight, Nicholas J. Terrill, Angelo Karunaratne, Fernando Cacho-Nerin, Martin M. Knight, and Himadri S. Gupta. The secret life of collagen: Temporal changes in nanoscale fibrillar pre-strain and molecular organization during physiological loading of cartilage. *ACS Nano*, 11(10):9728–9737, 2017. PMID: 28800220.

[83] José Antonio Jofre-Reche, Jérôme Pulpytel, Houssam Fakhouri, Farzaneh Arefi-Khonsari, and José Miguel Martín-Martínez. Surface treatment of polydimethylsiloxane (pdms) with atmospheric pressure rotating plasma jet. modeling and optimization of the surface treatment conditions. *Plasma Processes and Polymers*, 13(4):459–469, 2016.

[84] M. Lamblet, E. Verneuil, T. Vilmin, A. Buguin, P. Silberzan, and L. Léger. Adhesion enhancement through micropatterning at polydimethylsiloxane-acrylic adhesive interfaces. *Langmuir*, 23(13):6966–6974, 2007. PMID: 17511481.

[85] Marc-Antoine Campeau, Audrey Lortie, Pierrick Tremblay, Marc-Olivier Béliveau, Dominic Dubé, Ève Langelier, and Léonie Rouleau. Effect of manufacturing and experimental conditions on the mechanical and surface properties of silicone elastomer scaffolds used in endothelial mechanobiological studies. *BioMedical Engineering OnLine*, 16(1):90, Jul 2017.

[86] Melissa M. Basil-Jones, Richard L. Edmonds, Gillian E. Norris, and Richard G. Haverkamp. Collagen fibril alignment and deformation during tensile strain of leather: A small-angle x-ray scattering study. *Journal of Agricultural and Food Chemistry*, 60(5):1201–1208, 2012. PMID: 22233427.

[87] Knörzer E Nemetschek-Gansler H Nemetschek T Koch MH. Mosler E, Folkhard W. Stress-induced molecular rearrangement in tendon collagen. *J Mol. Biology*, 182(4):589–96, 1985.

[88] Hiroyuki Shima. Buckling of carbon nanotubes: A state of the art review. *Materials*, 5(1):47–84, 2012.

[89] Roger Hobbs, M S. Overington, J W. S. Hearle, and Stephen Banfield. Buckling of fibres and yarns within ropes and other fibre assemblies. *Journal of The Textile Institute - J TEXT INST*, 91:335–358, 01 2000.

[90] Samuel J. Baldwin, Laurent Kreplak, and J. Michael Lee. Characterization via atomic force microscopy of discrete plasticity in collagen fibrils from mechanically overloaded tendons: Nano-scale structural changes mimic rope failure. *Journal of the Mechanical Behavior of Biomedical Materials*, 60:356 – 366, 2016.

[91] K Misof, G Rapp, and P Fratzl. A new molecular model for collagen elasticity based on synchrotron x-ray scattering evidence. *Biophysical Journal*, 72, 1997.

[92] M. Tang, T. Li, and N.S. Gandhi. Heterogeneous nanomechanical properties of type 1 collagen in longitudinal direction. *Biomech Model Mechanobiol*, 16:1023–1033, 2017.

[93] Bryan D. Quan and Eli D. Sone. Structural changes in collagen fibrils across a mineralized interface revealed by cryo-tem. *Bone*, 77:42 – 49, 2015.

[94] Jared L. Zitnay, Yang Li, Zhao Qin, Boi Hoa San, Baptiste Depalle, Shawn P. Reese, Markus J. Buehler, S. Michael Yu, and Jeffrey A. Weiss. Molecular level detection and localization of mechanical damage in collagen enabled by collagen hybridizing peptides. *Nature Communications*, 8, 2017.

Appendix A

Additional Figures

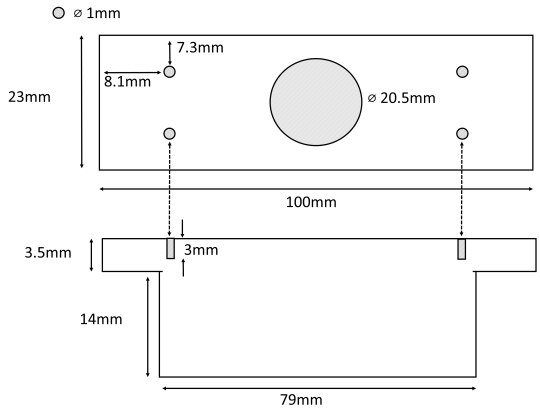

Figure A.1: *The stage-extension on which two motors were attached to strain a PDMS strip with adsorbed collagen fibrils. A 2cm-diameter hole, drilled perpendicular to the direction motor travel, allows for a long working-distance microscope objective to observe the strained PDMS from the bottom-up.*

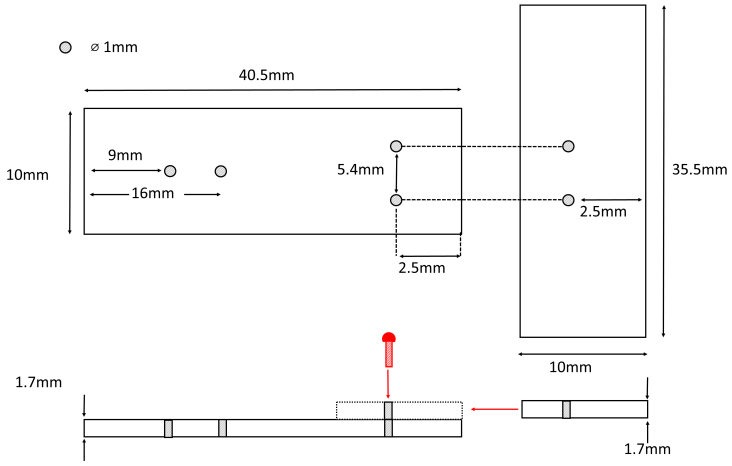

Figure A.2: *A clamp installed on each of the two motors, used to hold each end of the PDMS strip. The side-clamp used to hold the glass slide beneath the PDMS strip is fixed to the wide section of this clamp.*

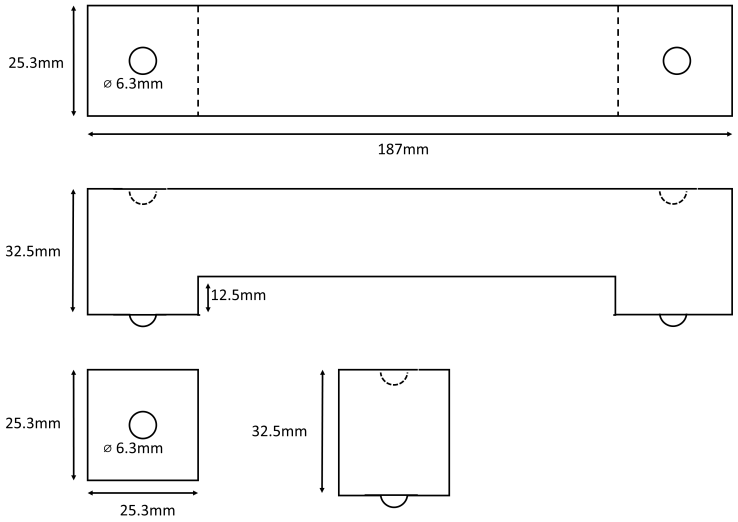

Figure A.3: n
A pair of stilts used to displace the AFM header vertically by 3.25cm, to make room for the motorized clamps holding the sample. These pieces were necessary for the cantilever to engage the sample, due to the limited working distance of the header.

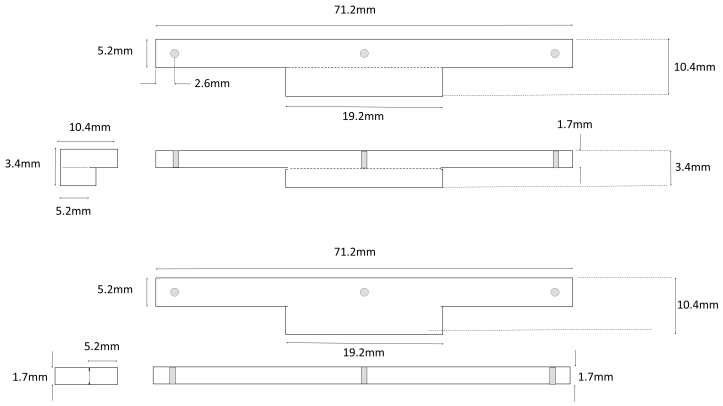

Figure A.4: *A side-clamp used to support a glass microscope cover-slip placed underneath the suspended PDMS strip during nanomechanical mapping. Without this cover slip to support the PDMS, the AFM cannot scan the PDMS surface in any form of contact mode due to induced oscillations of the free-standing film.*

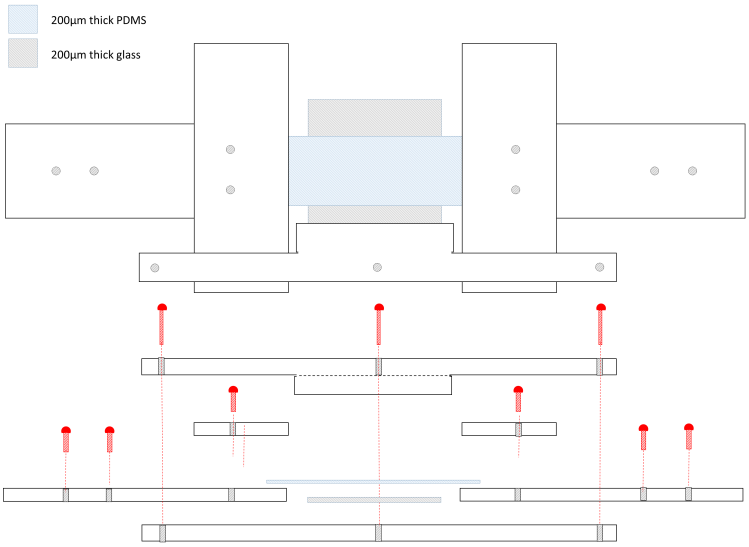

Figure A.5: *The motor clamps and glass clamp assembled in the configuration used during AFM imaging. Below is a side-view of the assembled piece.*

Appendix B

Copyright permission

Journal of cell science

Order detail ID:71930534
Order License Id:4615930145077
ISSN:1477-9137
Publication Type:e-Journal
Volume:
Issue:
Start page:
Publisher:COMPANY OF BIOLOGISTS LTD.
Author/Editor: Company of Biologists

Permission Status: **Granted**

Permission type: Republish or display content
Type of use: Republish in a thesis/dissertation

Requestor type	Academic institution
Format	Electronic
Portion	chart/graph/table/figure
Number of charts/graphs/tables/figures	1
The requesting person/organization	Chris Peacock
Title or numeric reference of the portion(s)	Figure 2
Title of the article or chapter the portion is from	Procollagen trafficking, processing and fibrillogenesis
Editor of portion(s)	N/A
Author of portion(s)	Elizabeth G. Canty
Volume of serial or monograph	N/A
Page range of portion	1344
Publication date of portion	March 23, 2005
Rights for	Main product
Duration of use	Life of current edition
Creation of copies for the disabled	no
With minor editing privileges	yes
For distribution to	Canada
In the following language(s)	Original language of publication
With incidental promotional use	no
Lifetime unit quantity of new product	Up to 499
Title	Structure and mechanics of stretched collagen fibrils
Institution name	Dalhousie University
Expected presentation date	Jul 2019

ELSEVIER LICENSE
TERMS AND CONDITIONS

Jun 25, 2019

This Agreement between Dalhousie University -- Chris Peacock ("You") and Elsevier ("Elsevier") consists of your license details and the terms and conditions provided by Elsevier and Copyright Clearance Center.

License Number	4615931086882
License date	Jun 25, 2019
Licensed Content Publisher	Elsevier
Licensed Content Publication	Journal of Structural Biology
Licensed Content Title	Fibrillar Structure and Mechanical Properties of Collagen
Licensed Content Author	Peter Fratzl,Klaus Misof,Ivo Zizak,Gert Rapp,Heinz Amenitsch,Sigrid Bernstorff
Licensed Content Date	Jan 1, 1998
Licensed Content Volume	122
Licensed Content Issue	1-2
Licensed Content Pages	4
Start Page	119
End Page	122
Type of Use	reuse in a thesis/dissertation
Intended publisher of new work	other
Portion	figures/tables/illustrations
Number of figures/tables/illustrations	1
Format	electronic
Are you the author of this Elsevier article?	No
Will you be translating?	No
Original figure numbers	Figure 3
Title of your thesis/dissertation	Structure and mechanics of stretched collagen fibrils
Publisher of new work	Dalhousie University
Expected completion date	Jul 2019
Estimated size (number of pages)	1
Requestor Location	Dalhousie University 6319 Pepperell St. Halifax, NS B3H 2P2 Canada Attn: Dalhousie University
Publisher Tax ID	GB 494 6272 12

ELSEVIER LICENSE
TERMS AND CONDITIONS

Jun 25, 2019

This Agreement between Dalhousie University -- Chris Peacock ("You") and Elsevier ("Elsevier") consists of your license details and the terms and conditions provided by Elsevier and Copyright Clearance Center.

License Number	4615940251658
License date	Jun 25, 2019
Licensed Content Publisher	Elsevier
Licensed Content Publication	Biophysical Journal
Licensed Content Title	Viscoelastic Properties of Isolated Collagen Fibrils
Licensed Content Author	Zhilei Liu Shen,Harold Kahn,Roberto Ballarini,Steven J. Eppell
Licensed Content Date	Jun 22, 2011
Licensed Content Volume	100
Licensed Content Issue	12
Licensed Content Pages	8
Start Page	3008
End Page	3015
Type of Use	reuse in a thesis/dissertation
Intended publisher of new work	other
Portion	figures/tables/illustrations
Number of figures/tables/illustrations	1
Format	electronic
Are you the author of this Elsevier article?	No
Will you be translating?	No
Original figure numbers	Figure 1
Title of your thesis/dissertation	Structure and mechanics of stretched collagen fibrils
Publisher of new work	Dalhousie University
Expected completion date	Jul 2019
Estimated size (number of pages)	1
Requestor Location	Dalhousie University 6319 Pepperell St. Halifax, NS B3H 2P2 Canada Attn: Dalhousie University
Publisher Tax ID	GB 494 6272 12

JOHN WILEY AND SONS LICENSE TERMS AND CONDITIONS

Jun 25, 2019

This Agreement between Dalhousie University -- Chris Peacock ("You") and John Wiley and Sons ("John Wiley and Sons") consists of your license details and the terms and conditions provided by John Wiley and Sons and Copyright Clearance Center.

License Number	4615931353277
License date	Jun 25, 2019
Licensed Content Publisher	John Wiley and Sons
Licensed Content Publication	Macromolecular Bioscience
Licensed Content Title	Micromechanical Testing of Individual Collagen Fibrils
Licensed Content Author	Joost A. J. van der Rijt, Kees O. van der Werf, Martin L. Bennink, et al
Licensed Content Date	Sep 28, 2006
Licensed Content Volume	6
Licensed Content Issue	9
Licensed Content Pages	6
Type of use	Dissertation/Thesis
Requestor type	University/Academic
Format	Electronic
Portion	Figure/table
Number of figures/tables	1
Original Wiley figure/table number(s)	Graphical Abstract
Will you be translating?	No
Title of your thesis / dissertation	Structure and mechanics of stretched collagen fibrils
Expected completion date	Jul 2019
Expected size (number of pages)	1
Requestor Location	Dalhousie University 6319 Pepperell St. Halifax, NS B3H 2P2 Canada Attn: Dalhousie University
Publisher Tax ID	EU826007151
Total	0.00 CAD
Terms and Conditions	

TERMS AND CONDITIONS

This copyrighted material is owned by or exclusively licensed to John Wiley & Sons, Inc. or one of its group companies (each a"Wiley Company") or handled on behalf of a society with which a Wiley Company has exclusive publishing rights in relation to a particular work